Coiled-coil biomaterials for biological applications

Shen, M.

Chapter 3

Investigating the Effect of Peptide Length on Coiled-Coil Stability, Self-Assembly, and Fusogenicity

ABSTRACT

Developing efficient drug delivery methods is challenging, as many rely on the endocytosis pathway to deliver drugs into cells. Unfortunately, the drug release efficiency is often low due to poor lysosomal/endosomal escape. Previously, we developed an efficient drug delivery system based on membrane fusion triggered by coiled-coil peptides to ensure cytosolic delivery of drugs. In this chapter, we investigate the effects of altering the lengths of the coiled-coil forming peptides K_n $(KIAALKE)_n$ and E_n $(EIAALEK)_n$ on membrane fusion. The secondary structure of the peptides was studied and it was found that long peptides (*i.e.* four or five heptads) tend to form homodimers. Also, K_5 and E_5 were found to form higher-order assemblies. Thermal stability studies showed that longer peptides, in both homo- and hetero-assemblies, are more stable than shorter peptides. Liposome membrane fusion assays revealed that the K_4/E_5 coiled-coil pair was optimal in triggering both lipid and content-mixing. Cell-liposome fusion experiments suggested that the K_4/E_4 coiled-coil pair was the most efficient at delivering the model drug propidium iodide (PI) into the cytosol of cells. In summary, this work studied the relationship between coiled-coil stability and peptide fusogenicity and provided further insights into the coiled coil-based membrane fusion system, which may have applications in drug delivery.

INTRODUCTION

Membrane fusion systems have potential applications in drug delivery.[1-3] Traditional drug delivery systems often rely on endosomal escape pathways and an inherent weakness is that the majority of the drug is either degraded or cleared after cell uptake due to lysosomal recycling pathways.[4-6] Therefore the membrane fusion pathway, which permits the direct delivery of molecules into cells, is considered a superior method as it avoids lysosomal pathways resulting in enhanced drug delivery efficiency.[3]

Membrane fusion is a fundamental, widespread process occurring in all cells. Full membrane fusion is characterized by both lipid mixing of the two opposing membranes and content mixing. The process usually contains the following steps: the opposing membranes are forced in close proximity by a given driving force, followed by a 'stalk' intermediate, after which hemifusion occurs resulting in lipid mixing. Finally, a fusion pore is formed resulting in content mixing.[7] Many processes such as embryogenesis,[8-10] *in vivo* vesicular transport,[11-12] and enveloped virus infection[13-15] rely on the occurrence of membrane fusion. As scientists have learned from these natural processes, many artificial membrane fusion systems have been designed which are able to achieve vesicle-vesicle membrane fusion.[16-18] However, very few of these artificial membrane systems are capable of achieving cell-vesicle membrane fusion and are able to deliver molecules into cells.[3, 19]

Coiled coils, a common folding motif in proteins, are widely used in biomaterial design.[20-24] A coiled coil consists of two or more α-helical peptides that are wrapped around each other to form a left-handed supercoil. Due to their folding properties and responsiveness, coiled coil-based building blocks are attractive for developing self-assembling, responsive, and bioactive materials.[21, 25-28]

In previous studies from our group, a coiled coil driven membrane fusion system has been designed.[29-30] The complementary coiled-coil forming peptides K and E were modified with a cholesterol membrane anchor connected via a PEG spacer, (denoted CPK and CPE), which readily insert into a synthetic or biological lipid membrane. By mixing CPK- and CPE-containing liposomes, efficient membrane fusion was achieved. A previous study showed that the liposome membrane fusion efficiency is correlated to coiled-coil stability.[31] For example, cell-liposome membrane fusion assays show that full membrane fusion can be achieved using four-heptad lipopeptides CPK_4 and CPE_4, while only cell-liposome docking was

achieved using three-heptad lipopeptides CPK_3 and CPE_3.[3, 32-34] Therefore, a more stable coiled-coil comprised of peptides with an additional heptad repeat unit may have an even better capacity to induce membrane fusion. Here, we have designed and synthesized the five heptad coiled-coil forming peptides K_5 and E_5. Using circular dichroism (CD) spectroscopy and dynamic light scattering (DLS), we studied the secondary structure, thermostability, and self-assembly of these coiled-coil forming peptides. The membrane fusion efficiency was evaluated by performing lipid and content mixing assays. A cell membrane labelling assay proved that all of these 'K_n' lipopeptides, CPK_3, CPK_4 and CPK_5 can be used to decorate cell membranes. Moreover, we quantitively studied the cell membrane docking efficiency and selected coiled-coil pairs that may induce efficient cell membrane-liposome fusion. For this, the efficiency of delivery of propidium iodide (PI) into cells and nitrobenzoxadiazole (NBD) incorporation in the cell membrane was quantified. We studied the relevance between coiled-coil stability and membrane fusion efficiency, providing a method for predicting and selecting coiled coils which have the greatest potential for membrane fusion and drug delivery.

RESULTS AND DISCUSSION

1. Secondary structure determination and self-assembly of coiled-coil forming peptides K and E

The two complementary peptides used in this study are based on original designs from the Hodges group.[35] These two peptides are rich in lysine and glutamic acid and were named peptide K and peptide E respectively. Peptides K_n $(KIAALKE)_n$ and E_n $(EIAALKE)_n$ were designed to form a heterodimeric coiled-coil, by virtue of the residues that make up the hydrophobic core and their opposing charges.

In this study, we used either three, four or five heptads in E_n/K_n. All the peptides have a 'GW' extension at the C-terminus to facilitate accurate concentration determination (see methods). The sequences of all peptides used in this study are listed in Table 1. All lipopeptides used in this study do not contain the 'GW' tail at the C-terminus and so their concentration was calculated based on their weight.

Table 1. Coiled-coil forming peptides used in this study.

Peptides	Sequence						
	ef	*gabcdef*	*gabcdef*	*gabcdef*	*gabcdef*	*gabcdef*	*ga*
K_3		KIAALKE	KIAALKE	KIAALKE	GW		
E_3		EIAALEK	EIAALEK	EIAALEK	GW		
K_4		KIAALKE	KIAALKE	KIAALKE	KIAALKE	GW	
E_4		EIAALEK	EIAALEK	EIAALEK	EIAALEK	GW	
K_5		KIAALKE	KIAALKE	KIAALKE	KIAALKE	KIAALKE	GW
E_5		EIAALEK	EIAALEK	EIAALEK	EIAALEK	EIAALEK	GW
Flu-K_4[a]	Fluo-GG	KIAALKE	KIAALKE	KIAALKE	KIAALKE	GW	
Flu-E_4[a]	Fluo-GG	EIAALEK	EIAALEK	EIAALEK	EIAALEK	GW	

[a]Fluo-K_4 and Fluo-E4: 5(6)-Carboxyfluorescein conjugated peptide K_4 and peptide E_4.

CD spectroscopy was employed to study the secondary structure of the different coiled-coil forming peptides. In line with the previous study,[31] K_3 and E_3 adopt an unfolded secondary structure, while four and five heptad peptides show a typical helical structure (Figure 1A and Table 2). This is somewhat surprising because the peptides are designed to be unfolded on their own as the presence of charged residues means self-association is disfavored. However, for the longer peptides, the stabilization gained by burying the hydrophobic residues appears to outweigh the destabilizing effects of the repulsive electrostatic interactions. A previous study also showed that both peptides K and E are prone to form homodimers, inducing these peptides to form a helical structure.[36]

The ellipticity ratio between the minima at 222/208 nm can be used to determine whether isolated helices (<0.9) or coiled-coil (>1) structures are formed.[37-38] For all the four and five heptad peptides, the ellipticity ratios at 222/208 nm were > 1.15, suggesting homodimer formation.

Figure 1B shows the thermal melting curves of all peptides. As expected, longer peptides are more stable when heated from 5 to 90°C, reflecting the higher melting temperature (T_m) (Table 2). When comparing peptides with the same number of heptads, the K_4/K_5 peptides are more stable than E_4/E_5 peptides, which is in line with the previous observation that peptide K forms more stable homodimers than peptide E.[39]

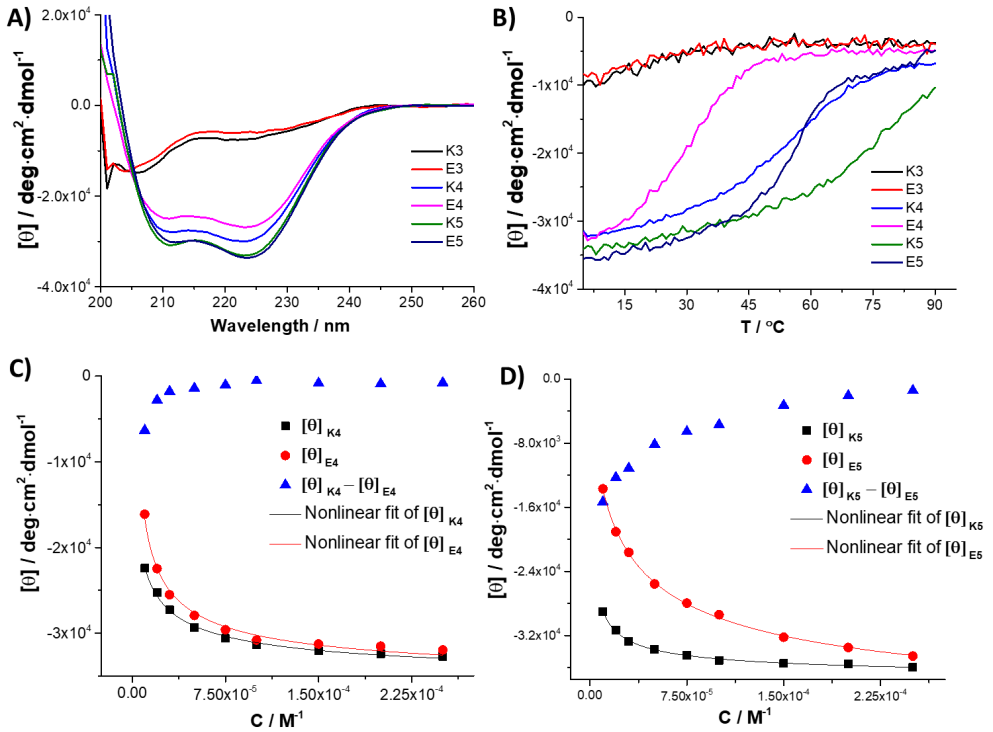

Figure 1. (A) CD spectra of peptides K_n and E_n. (B) Thermal melting curves for the different peptides. (C) Concentration-dependent CD titration of peptides K_4 and E_4. (D) Concentration-dependent CD titration of peptides K_5 and E_5. The non-linear fit curves were obtained based on equation 6. All measurements were performed in PBS (pH 7.2). [Peptide] = 10 μM. All measurements except the melting curve were recorded at 20 °C.

Table 2 Characteristics of peptides K and E with differing numbers of heptads as measured by CD spectroscopy.

	K_3	E_3	K_4	E_4	K_5	E_5
Helicity / % [a]	26	22	89	80	95	96
$[\theta]_{222}$ / $[\theta]_{208}$	0.55	0.50	1.20	1.15	1.22	1.30
Helicity decline / %	62	53	78	85	70	86
T_m / °C [b]	-	-	50	34	77	55

[a]The helicity of all peptides was calculated using equation 5. [b] The T_m was obtained by calculating the first-order derivative of the melting curve using the JASCO spectra analysis software, in which the melting temperature corresponds to the peak maximum of the first-order derivative.

To study homodimer formation of four and five heptad peptides, a titration assay

was performed using CD spectroscopy. Figure 1C shows the CD titration results for the four heptad peptides K_4 and E_4. A non-linear correlation between peptide molar ellipticity and concentration was obtained,[40] revealing that the homodimer is formed in a concentration-dependent manner. The difference in molar ellipticity between peptides K_4 and E_4, as a function of concentration, is remarkable at low concentrations (Figure 1C), while there is almost no difference at high concentrations. This suggests that peptide K_4 forms a homodimer more readily than E_4 at low peptide concentrations. At high peptide concentrations, both peptides tend to homodimerize. For K_5 and E_5, the same trend was observed (Figure 1D). The molar ellipticity of peptide K_5 is consistent at different concentrations, suggesting that homodimer formation occurs at all measured concentrations. In contrast, the helicity of peptide E_5 is strongly concentration-dependent. At high peptide concentrations, peptides K_5 and E_5 have a similar molar ellipticity, suggesting that both peptides are fully homodimerized with a helicity of ~96%. It should be noted that, although the non-linear curve fitting (obtained by equation 14) matches well to the CD data (Figure 1C & 1D), the dissociation constant (K_d) of these peptides could not be determined as the peptides are not fully unfolded even at very low concentrations.

2. Concentration-dependent thermal stability of peptides K_5 and E_5

The thermal stability and concentration-dependent CD titration studies suggest homodimer formation of peptides K_5 and E_5. To further study this, temperature-dependent CD measurements were performed to evaluate the thermal stability of peptides K_5 and E_5 at different concentrations (Figure 2A and 2B). The melting temperature (T_m) was calculated based on the first-order derivative of the melting curve (Figure 2C). For K_5, the T_m increases by 10 °C when the peptide concentration increases from 3 μM to 9 μM, suggesting concentration-dependent thermal stability. Surprisingly, the T_m decreased 5 °C when the peptide concentration was increased further to 12 μM. To investigate whether this could be caused by peptide aggregation, we performed DLS measurements. Indeed, with increasing temperature, the derived count rate (DCR) increased, suggestive of peptide K_5 aggregates at high temperatures. A higher peptide concentration is likely to contribute to the peptide aggregate formation, leading to the apparent T_m decrease of K_5 at a higher concentration. For peptide E_5, a continuous, yet small T_m increase was obtained when the peptide concentration was increased from 3 μM to 12 μM. Since the DCR remained stable as the temperature was increased, it

suggests that E_5 does not aggregate.

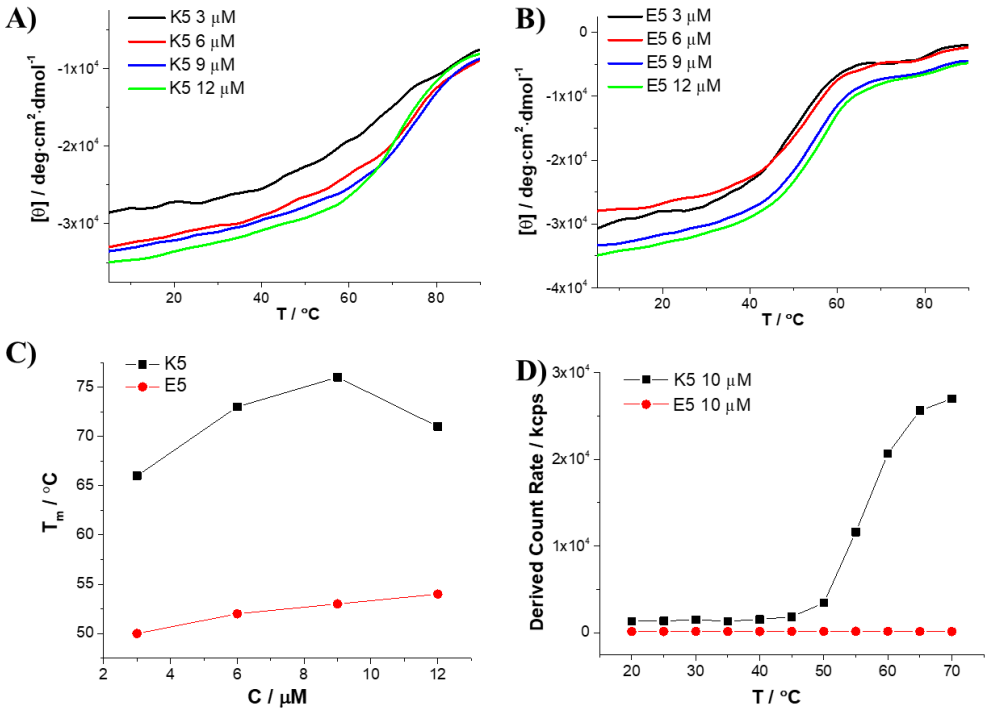

Figure 2. Melting curves of peptide K_5 (A) and E_5 (B) at a different peptide concentration, (C) correlation of peptide melting temperature (T_m) to the peptide concentration, (D) temperature-dependent DCR of peptide K_5 and E_5, measured by DLS. All measurements were recorded in PBS (pH 7.2).

3. Thermal stability of peptides K_5 and E_5 in the presence of GdnHCl

Both K_5 and E_5 were found to be highly thermally stable. To further understand the stability of peptides K_5 and E_5, guanidine hydrochloride (GdnHCl) was used to study the peptide folding stability. GdnHCl is a commonly used protein denaturing reagent of which the mechanism of denaturation is still controversial.[41-43] The generally accepted theory is that GdnHCl affects electrostatic interactions.

Different concentrations of GdnHCl were added to the peptides and the melting curves were measured by CD spectroscopy. It should be noted that the high UV-Vis absorption of GdnHCl can influence the CD spectra at wavelengths < 215 nm (Figure S1), fortunately, the typical α-helix maximum at 222 nm is not affected (Figure S2), which makes monitoring of the peptide unfolding possible. The results show that increasing the concentration of GdnHCl indeed impacts the thermal

stability of both K_5 and E_5, as evidenced by the shift in T_m. Interestingly, in the presence of 1M and 3M GdnHCl the T_m of both K_5 and E_5 increased (Figure 3A & 3B) with the highest T_m for both peptides was found at 1M GdnHCl. For K_5, the T_m decreased (relative to the peptide in the absence of GdnHCl) only when 5M GdnHCl was present. Remarkably, even in 5 M GdnHCl, E_5 is still more stable than in the absence of this reagent. One explanation for this behavior is that at a low concentration of GdnHCl, the Gdn^+ can bind to the negatively charged glutamic acid residues eliminating the charge interactions between peptides. Such a result could contribute to homodimer formation and increase the thermostability of peptides K_5 and E_5. At high concentrations, GdnHCl acts as a classical denaturant that unfolds and destabilizes the peptides, which results in a decrease of the T_m for both peptides. In addition, temperature-dependent K_5 peptide aggregation was not observed in the presence of GdnHCl (Figure 3D).

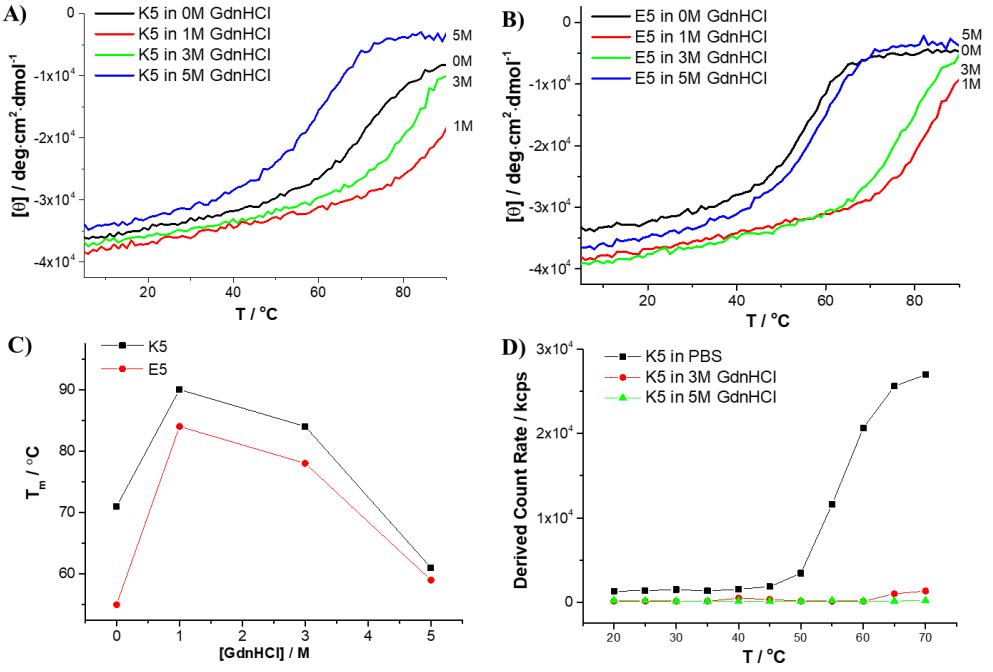

Figure 3. CD melting curves of K_5 (A) and E_5 (B) in the presence of GdnHCl at different concentrations. (C) Correlation of peptide melting temperature (T_m) to GdnHCl concentration. (D) Temperature-dependent DLS study of the effect of GdnHCl on K_5 peptide aggregation formation. Spectra were recorded in PBS (pH 7.2). [Peptide] = 10 μM.

This study shows that GdnHCl influences the thermostability of both peptide K_5 and E_5, possibly by influencing the electrostatic interactions between peptides,

impacting homodimer formation. To study homodimer formation of K_5 and E_5 in the presence of GdnHCl, thermal unfolding experiments were performed at different peptide concentrations in the presence of 3 M or 5 M GdnHCl (Figure 4A & 4B). Next, the T_m was calculated for each melting curve (Figure 4C & 4D). The T_m increased with increasing peptide concentration, suggesting that homodimer formation is still possible in presence of GdnHCl. This suggests that the hydrophobic interactions may not be influenced by the addition of GdnHCl. Moreover, GdnHCl at 3 M seems to decrease the electrostatic interactions between peptides or reduce the repulsion between peptides (for peptide E_5) thus contributing to the stability of the homodimeric coiled-coil.

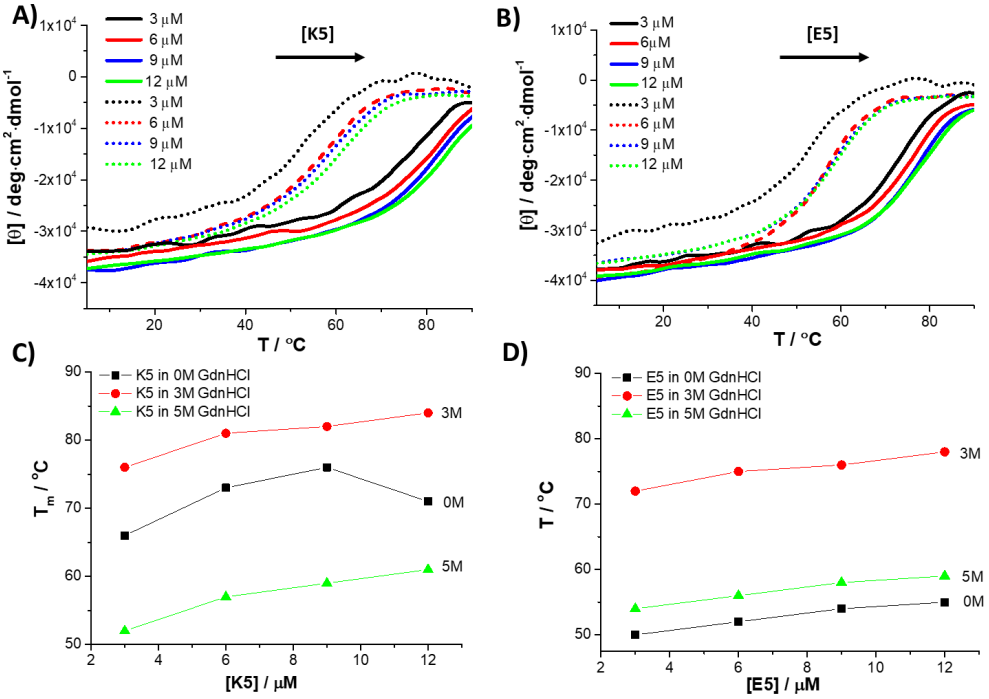

Figure 4. CD melting curves for different concentrations of K_5 (A) and E_5 (B) in presence of 3 M (solid lines) or 5 M (dotted lines) GdnHCl. (C) Correlation of T_m for K_5 (C) and E_5 (D) to peptide concentration with 0 M, 3 M and 5 M GdnHCl. Spectra were recorded in PBS (pH 7.2).

4. E/K coiled coils: thermal stability and self-assembly

Heterodimeric coiled-coil formation of three-, four- and five-heptad peptides was also studied and evaluated by CD spectroscopy (Figure 5A and Table 3). Upon mixing, the unfolded K_3 and E_3 form a helical structure with a high overall helicity

and T_m indicating the peptides form a heterodimeric coiled-coil. A helicity increase was also obtained for the K_4/E_4 mixture, indicating coiled-coil formation. However, no helicity increase was obtained when peptides K_5 and E_5 were mixed because these peptides were nearly fully helical already. An increase in the 222/208 nm ellipticity ratio was achieved, which suggests coiled-coil formation. Support for this comes from the thermal melting experiment of K_5/E_5 as the thermostability increased (Figure 5B).

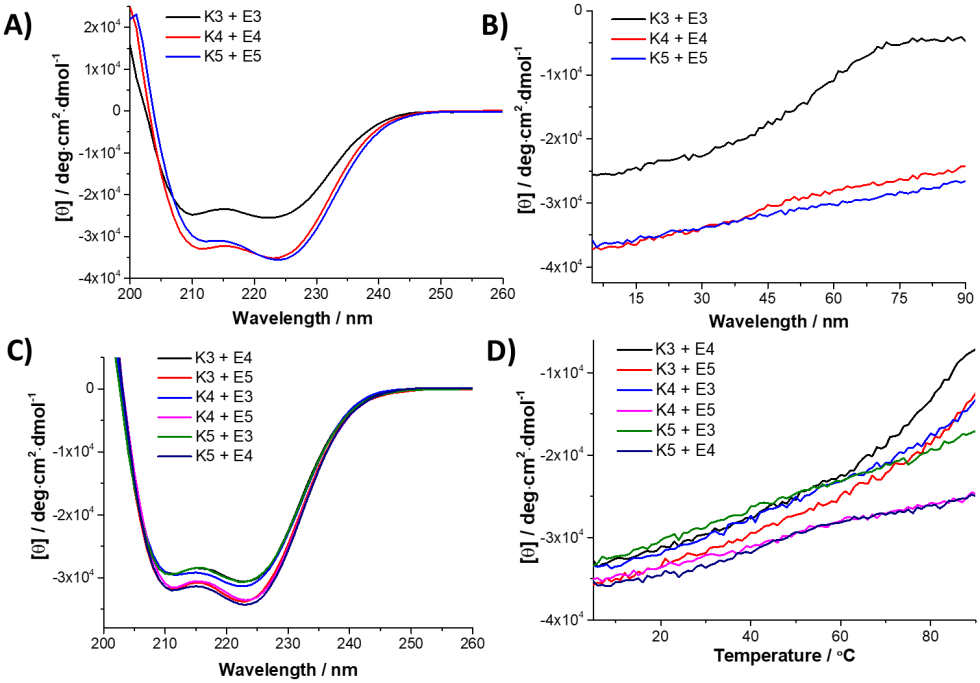

Figure 5. CD spectra of symmetric (A) and asymmetric (C) coiled-coil peptide pairs. CD melting curves of symmetric (B) and asymmetric (D) coiled-coil peptide pairs. All measurements were performed in PBS (pH 7.2) with [peptide] = 10 μM at 20 °C.

Table 3. Characteristics of coiled coils formed by combining E and K peptides of different lengths.

Entry	K_3-E_3	K_4-E_4	K_5-E_5	K_3-E_4	K_3-E_5	K_4-E_3	K_4-E_5	K_5-E_3	K_5-E_4
Helicity / %	72	96	95	85	99	87	91	85	93
$[\theta]_{222}$ / $[\theta]_{208}$	1.10	1.21	1.40	1.16	1.19	1.19	1.23	1.15	1.21
Helicity Decline / %	82	35	26	78	66	60	30	49	29
T_m / °C	58	> 90	> 90	77	> 90	> 90	> 90	> 90	> 90

Asymmetric coiled-coil pairs were also evaluated (Figure 5C and Table 3). Generally, a higher total number of heptad repeats results in a higher helicity of the coiled-coil complex. The thermal stability study reveals that all these coiled-coils have a high thermostability which correlated to the total number of heptad repeats (Figure 5D).

To determine whether high-order assemblies were formed in a mixture of K_5/E_n mixture, DLS experiments were performed to determine the DCR (Figure 6A). For all the individual peptides and all coiled-coil pairs (except for K_5), a low DCR was observed indicative of the absence of large aggregates. Peptide K_5 and K_5/E_n coiled-coils showed only a threefold increase of the DCR in comparison to other peptide monomers, revealing that they tend to form self-assembled peptide aggregates in solution. However, a > 100 fold in the DCR was observed for the K_5/E_5 coiled-coil pair. UV-Vis measurements also indicated particle formation of the K_5-E_5 coiled-coil pair (Figure S3). We speculate that a mismatched, or 'slipped' structure may form in the K_5/E_5 complex due to the long hydrophobic face, resulting in exposed hydrophobic residues inducing the formation of large assemblies. Next, a temperature-dependent DLS assay was performed. The DCR decreased upon increasing the temperature, revealing that K_5/E_5 assemblies are temperature sensitive (Figure 6B). Interestingly, no DCR increase was obtained when the solution was cooled from 90 °C back to 20 °C, indicating that these larger assemblies are kinetic products. We, therefore, hypothesize that large assemblies are formed as a result of slipped coiled-coil formation. However, these assemblies are less stable than an aligned heterodimeric assembly. By increasing the temperature, these kinetically trapped assemblies dissolve and the thermodynamically stable blunt-ended coiled-coil is obtained.

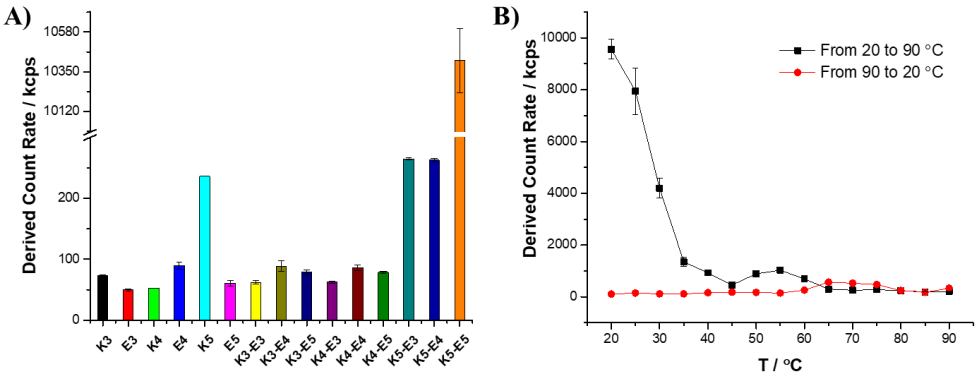

Figure 6. (A) DCR determined by DLS measurements to probe the self-assembly of different peptides and coiled coils at 20 °C. (B) Temperature-dependent DCR of K_5-E_5. The temperature changes at a rate of 1 °C/min and the measurement of each data point takes ~5 minutes. All measurements were recorded in PBS (pH 7.2) with a peptide concentration of 10 µM.

Next, the thermal stability of E_5/K_5 was determined in the presence of GdnHCl. With increasing concentrations of GdnHCl, the thermostability of the coiled-coil complex decreases gradually, as anticipated (Figure 7A & 7B). Due to the high thermal stability of the E_5/K_5 pair, the T_m cannot be accurately determined and was estimated when the GdnHCl concentration was lower than 4 M. The unfolded state of the E_5/K_5 complex was reached only in the presence of 5 M GdnHCl. This differs from the monomer peptides K_5 or E_5 which showed optimal thermal stability at a low GdnHCl concentration (*i.e.* 1 M and 3 M). This further verified our hypothesis that GdnHCl mainly influences the electrostatic interactions between lysines and glutamic acids in heterodimeric coiled coils, thus decreasing the thermal stability.

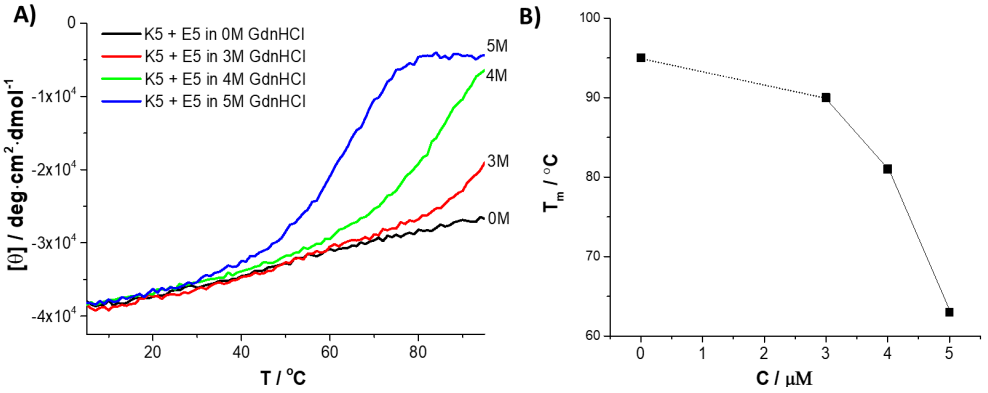

Figure 7. (A) CD melting curves of the K_5-E_5 coiled coil with different concentrations of GdnHCl. (B) Correlation of the K_5-E_5 coiled coil T_m to GdnHCl concentration. All measurements were recorded in PBS (pH 7.2). [K_5 + E_5] = 5 µM + 5 µM.

5. Lipid mixing and content mixing using lipopeptides CPK_n and CPE_n

Liposome membrane fusion represents the process where two vesicles are forced to be close to each other, and then adopt a hemifusion state where lipid mixing occurs, following by content mixing as the final step. Previous studies have shown that the efficiency of K/E induced membrane fusion is related to many factors, including coiled-coil stability.[30-31, 40, 44] The K_5/E_5 coiled-coil pair is more stable than the previously tested pairs and therefore the fusogenicity was studied by performing lipid-mixing and content-mixing assays.

A lipid mixing assay was performed using the Förster resonance energy transfer (FRET) pair of NBD/lissamine rhodamine B (LrB).[30, 40] The NBD-PE and LrB-PE dyes were incorporated into liposomes. Before lipid mixing, the NBD (donor) and LrB (acceptor) fluorophores are in close proximity resulting in FRET and thus a weak NBD emission. When fusion occurs with plain liposomes (*i.e.* liposomes without fluorophores), the average distance between NBD and LrB increases, with concomitant NBD emission increase. Here, nine symmetrical and non-symmetrical coiled-coil combinations were investigated for their ability to promote lipid mixing (Figure 8A-C). The four and five heptad coiled-coil pairs show a higher lipid mixing efficiency than coiled coils containing three heptad peptides, indicating that membrane fusion efficiency is related to coiled-coil stability. Interestingly, the K_5-E_4 coiled coil showed the highest lipid mixing efficiency while the K_5-E_5 coiled coil shows only the fourth-highest lipid mixing efficiency, which suggests that coiled-coil stability is not the only factor determining fusogenicity. Further analysis

of the lipid mixing efficiency (Figure S4A) revealed that by increasing the length of peptide K, lipid mixing also increased. These results support the theory that peptide K plays a crucial role in membrane fusion, whilst the E peptide plays more of a supporting role.[45-46]

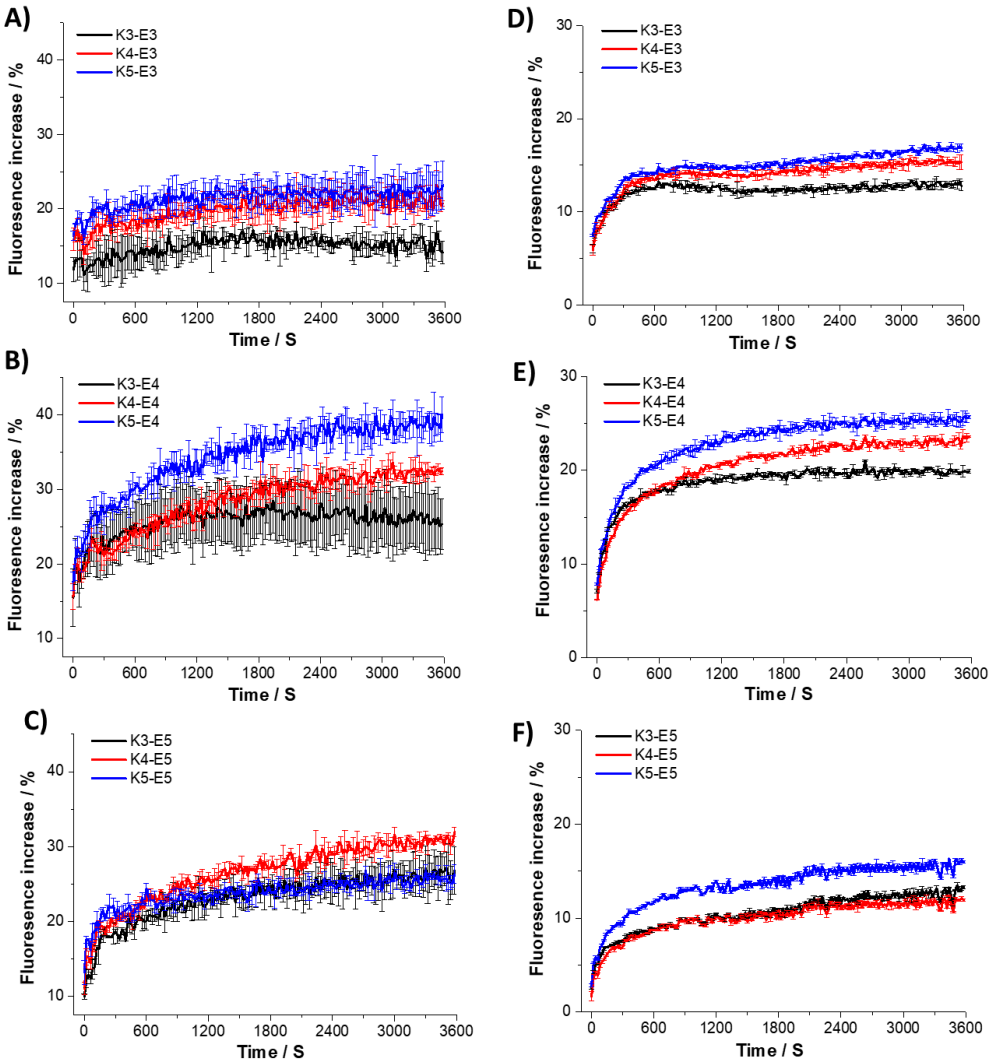

Figure 8. Lipid mixing assays triggered by K_n-E_3 (A), K_n-E_4 (B) and K_n-E_5 (C) coiled-coil pairs (n=3-5). Content mixing assay performed using K_n-E_3 (D), K_n-E_4 (E) and K_n-E_5 (F) coiled-coil pairs.

Efficient content mixing is the hallmark of membrane fusion. For content mixing assays, Sulforhodamine B (SrB) at self-quenching concentrations was encapsulated

into liposomes. Upon fusion with plain liposomes, the SrB will be diluted resulting in a fluorescence increase (Figure 8D-F). The highest amount of membrane fusion was obtained with K_5-E_4, in line with the lipid mixing assay. The total content mixing efficiency analysis (Figure S4B) shows that the content mixing efficiency also increases when using the longer peptide K. For peptide E, the four heptad variant yielded the highest membrane fusion efficiency, while E_5 had the lowest efficiency. This might be due to the fact that peptide E_5 forms a stable homodimer, resulting in a low effective E_5 concentration available to interact with peptide K, resulting in a fusion efficiency decrease.

The overall results of lipid mixing and content mixing show that optimal membrane fusion was obtained using the K_5-E_4 pair. Together with the coiled-coil stability study, it can be concluded that although coiled-coil stability is important for membrane fusion, other factors such as the stability of homodimers and the presence of higher-order assemblies also influence liposome fusion efficiency.

6. Cell Membrane labelling

CPK_3 and CPK_4 were previously used to decorate cell membranes[3, 32] To determine whether CPK_5 is also able to modify cell membranes, a membrane labeling assay was performed. Cells were decorated with CPK_n and the binding of fluorescein labelled E_4 (fluo-E_4) through coiled-coil formation at the cell membrane was studied. As expected, all CPK_n were able to decorate cell membranes and interact with fluo-E_4 (Figure 9). The fluorescence intensity on the cell membrane increased when the cells were decorated with longer CPK_n, revealing the correlation with coiled-coil stability of K_n/E_n (Table 3).

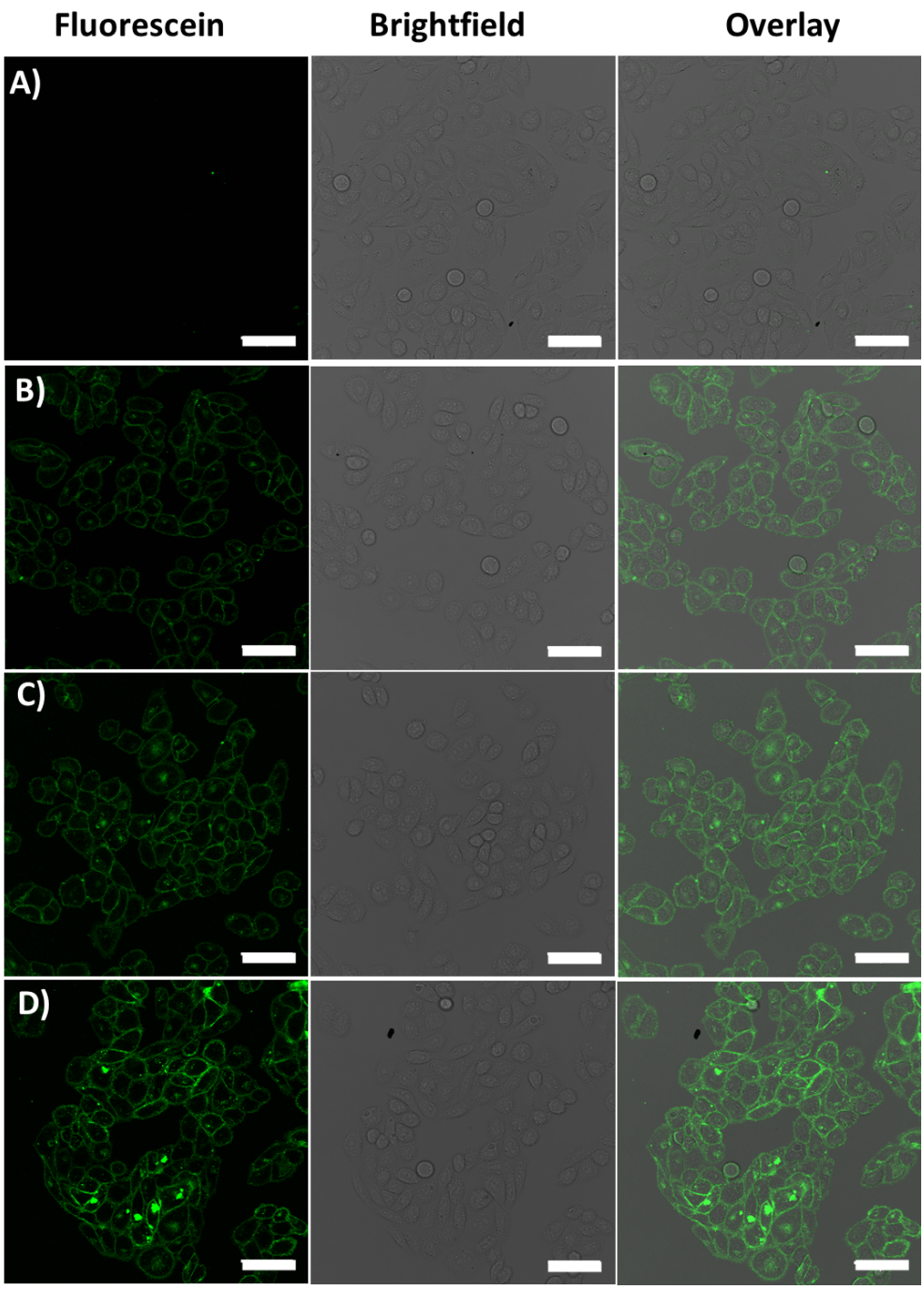

Figure 9. Cell membrane labelling assay. Non-CPK decorated cells incubated with fluo-E_4 (A). Cells incubated with 10 μM CPK_3 (B), CPK_4 (C) or CPK_5 (D) for two hours, following by incubated with fluo-E_4 (20 μM) for 10 minutes. Scale bar: 50 μm. Green: fluorescein.

7. Cell-liposome docking

To investigate cell-liposome membrane fusion triggered by the different coiled-coil pairs, cell-liposome docking was studied as a first step before full membrane fusion was performed.

Hela cells were decorated with CPK_n of varying lengths and treated with CPE_n liposomes labelled with NBD-PE. Cell-liposome docking was quantified using FACS and we determined both the percentage of fluorescent cells and also the mean fluorescence intensity per cell. Efficient fluorescent-labelling of cells with all coiled-coil pairs was observed (Figure 10A). In the absence of CPK_n, < 5% of cells were fluorescently labelled. The mean fluorescence intensity was also measured, showing that the cell-liposome docking efficiency is dependent on the coiled coil used (Figure 10B). Coiled-coils pairs formed by four- and five-heptad peptides exhibit higher mean fluorescence intensities. This might be because the three heptad peptides are shorter, thus coiled-coil formation is hindered due to steric hindrance, or because longer peptides form more stable coiled coils.

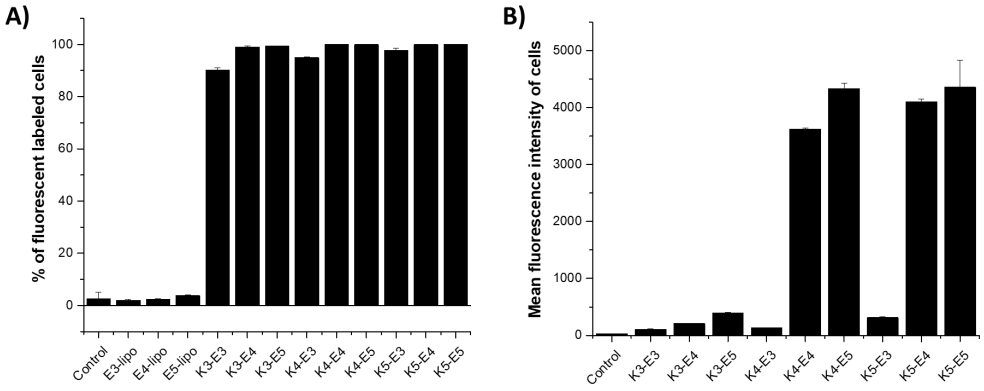

Figure 10. FACS analysis of cells in the cell-liposome docking assay induced by different coiled-coil pairs. (A) Analysis of fluorescent cells (A) and mean fluorescence intensity of fluorescent cells (B).

8. Cell-liposome membrane fusion

The liposome-cell docking assay illustrates that the four and five heptad peptides are most efficient at inducing liposome docking on cell membranes. Next, we investigated the fusogenicity of the coiled-coil pairs which achieved the highest cell-liposome docking. The K_3-E_3 coiled-coil pair was used as a reference. Propidium iodide (PI) is a membrane-impermeable dye, therefore it is a suitable

dye for studying cell-liposome membrane fusion as it cannot enter cells spontaneously.[3] Hela cells were decorated with CPK_n lipopeptides and treated with CPE_n liposomes containing PI. Upon fusion, the nucleus will be stained red. As expected, the CPK_3-CPE_3 coiled-coil pair led to low cell-liposome membrane fusion efficiency as only a weak fluorescence was observed on both the cell membrane and in the nucleus (Figure 11A). Optical cell-liposome fusion was obtained with CPK_n decorated cells and CPE_n liposomes (Figure 11B). Homogenously NBD-labelled cell membranes and a PI-stained cytosol and nucleus were observed. The CPK_4/CPE_5 pair also showed good delivery of PI to the cells (Figure 11C). In contrast, both CPK_5/CPE_4 and CPK_5/CPE_5 coiled-coil pairs showed strong NBD labelling of the cell membrane but weak PI staining (Figure 11D & 11E), resulting in efficient cell-liposome docking but low membrane fusion. Thus CPK_5 decorated cells are able to capture CPE_n modified liposomes efficiently (Figure 11D & 11E), but have limitations in completing fusion and releasing liposomal contents into cells. The CPE_4-modified liposomes did display an advantage over CPE_5-modified liposomes as more homogenous docking on the cell membrane was observed (Figure 11B *vs* 11C and 11D *vs* 11E). This might be due to the fact that CPE_5-modified liposomes contain more negative charges resulting in more repulsion with the negatively charged cell membrane.

The control experiments show that without CPK decoration on the cell membrane or CPE modification on the liposomes, neither cell-liposome docking nor cell-liposome fusion occurred (Figure S5 & S6). Because the lipid composition of a cell membrane is more complex than the liposome membrane, the final cell-liposome membrane fusion efficiency is not the same as the liposome-liposome membrane fusion. In summary, the K_4-E_4 coiled coil is optimal for cell-liposome fusion, while the K_5/E_4 pair is the best choice for liposome-liposome fusion.

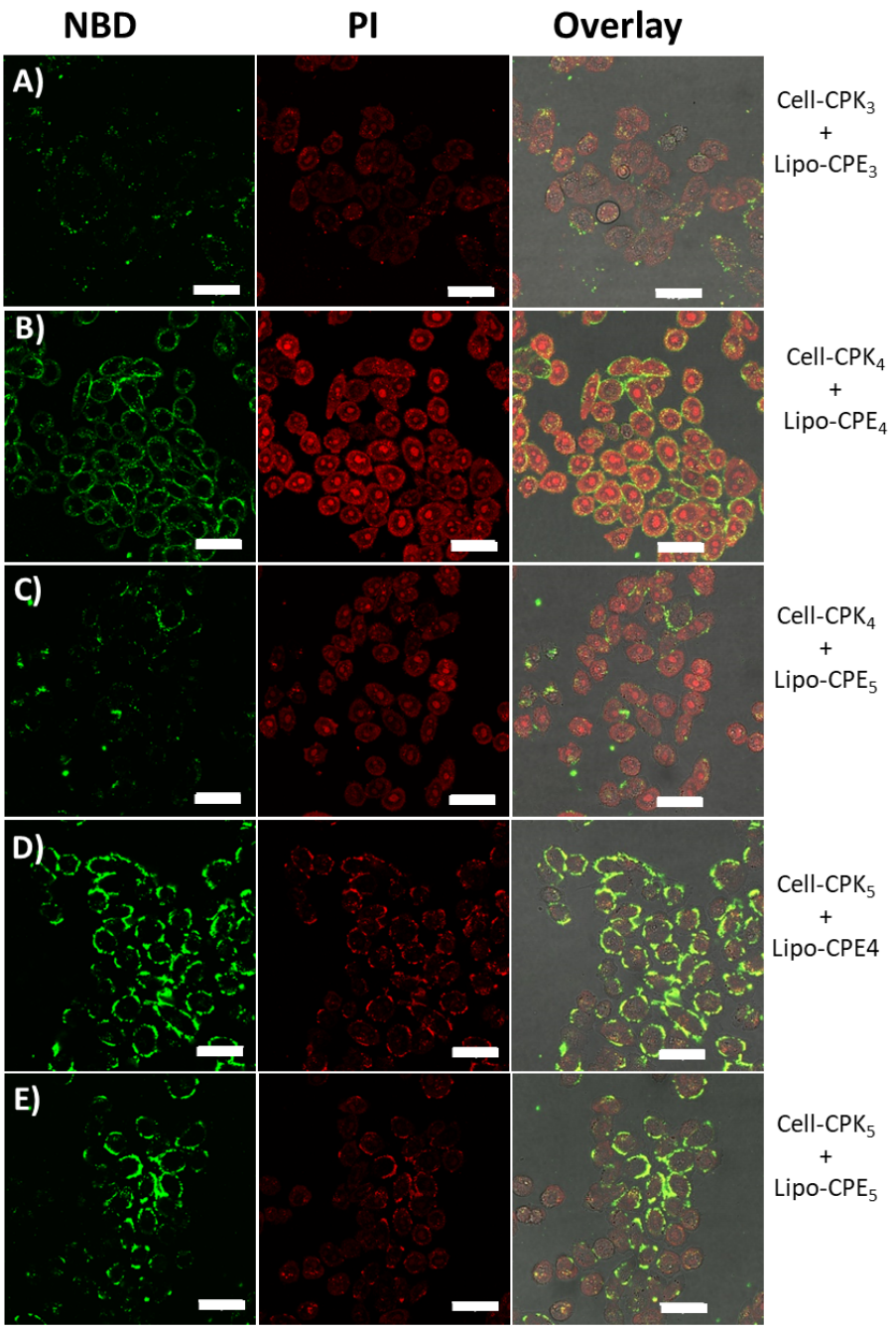

Figure 11. Cell-liposome fusion assay using CPK_n and CPE_n. Cells were treated with CPK_n lipopeptides (10 μM), followed by incubation with different CPE_n-modified liposomes (200 μM) which contained PI inside and NBD-PE on the lipid membrane. Scale bar: 50 μm. Green: NBD, red: PI.

CONCLUSION

In this work, six coiled-coil forming peptides with different numbers of heptad repeat units were designed, synthesized and evaluated. Using CD spectroscopy, the secondary structure of these individual peptides, as well as the heterodimeric coiled coils were studied. As expected, the longer peptides tend to be more helical. We also found that peptide K_5 self-assembles to form peptide aggregates at high temperatures but is soluble at low temperatures. In contrast, an equimolar E_5/K_5 mixture aggregates at low temperatures and becomes soluble at elevated temperatures. These results suggest a complicated self-assembly process for K_5 and the E_5/K_5 coiled coils. Thermal melting curves reveal that both K_5 and E_5 have concentration-dependent unfolding behavior, suggesting possible homodimer formation. The thermostability of K_5 and E_5 increases in the presence of 1M GdnHCl and decreases at higher GdnHCl concentrations. The stability of the E_5/K_5 coiled coil decreases as the GdnHCl concentration increases. This study suggests that GdnHCl may be able to weaken electrostatic interactions between amino acid side chains and influence peptide stability in this manner.

Six lipopeptides with different peptide lengths have been synthesized and membrane fusion assays were performed. The results show that the K_5-E_4 coiled-coil pair is optimal for inducing efficient lipid and content mixing. Cell membrane labeling assays prove that all CPK_n lipopeptides can decorate cell membranes and form coiled coils with the complimentary peptide E_4. By performing cell-liposome docking assays, we found that used of E_n/K_n (n = 4 or 5) coiled-coil pairs resulted in efficient membrane docking. A PI delivery assay suggests that the cell-liposome fusion efficiency was optimal using CPE_4/CPK_4. These results reveal that coiled-coil stability is relevant to membrane fusion, but the fusogenicity of coiled-coil peptides is also influenced by peptide self-assembly and membrane-peptide interactions.

Together, this data provides insights into the most effective coiled-coil pairs for membrane fusion, which may ultimately have applications in drug delivery.

EXPERIMENTAL SECTION

Chemical and Materials

All chemicals were supplied by Sigma and used without further purification unless otherwise stated. Amino acids were purchased from Novabiochem. Tentagel HL RAM resin was obtained from Iris Biotech GmbH. All solvents, as well as piperidine, trifluoroacetic acid, and acetic anhydride, were purchased from Biosolve. Oxyma pure was purchased from Carl Roth GmbH. All lipids were supplied by Avanti Polar Lipids. The Chambered Coverslips for confocal microscopy were purchased from Ibidi (µ-Slide 8 Well). Ultrapure water was obtained by a Milli-Q^{TM} purification system from Millipore (Amsterdam, the Netherlands).

Peptide synthesis

All peptides were synthesized on a CEM Liberty Blue microwave-assisted peptide synthesizer using Fmoc chemistry. 20% piperidine in DMF was used as the deprotection agent. During coupling, DIC was applied as the activator and Oxyma as the base. All peptides were synthesized on a Tentagel S RAM or HL RAM resin (0.39 mmol/g for K_3 and E_3, 0.22 mmol/g for K_4 and E_4, 0.19 mmol/g for K_5 and E_5). The resin was swollen for at least 15 min before use. For each amino acid coupling step, 5 equivalents of the Fmoc protected amino acid (2.5 mL in DMF), DIC (1 mL in DMF) and Oxyma (0.5 mL in DMF) were added to the resin in the reaction vessel and heated to 90 ℃ for 4 minutes. For each deprotection step, 20% of piperidine (4 mL in DMF) was used and heated to 90 ℃ for 1 minute. Between the deprotection and peptide coupling steps, the resin was washed three times using DMF. For the three heptad and four heptad peptides, a single coupling method was used for the synthesis. For five heptad peptides, the single coupling method was used for the first four heptads and a triple coupling method was used for the last heptad.

For peptides used in CD and DLS studies, the N-terminus of the peptides was manually acetylated. To the 0.1 mmol resin-loaded peptide, 3 mL DMF containing 5% acetic anhydride and 6% pyridine was added and shaken for 1 hour at room temperature.

For synthesis of fluo-K_4 and fluo-E_4, two additional glycine residues were coupled to the N-terminus of the peptides on resin, before fluorescein was manually

coupled by the addtion of 0.2 mmol 5(6)-carboxyfluorescein, 0.4 mmol HCTU and 0.6 mmol DIPEA in 3 mL DMF. The reaction was shaken at room temperature overnight.

For lipopeptide synthesis, a poly(ethylene glycol) $(PEG)_4$ linker and cholesterol were coupled manually to the peptide on-resin. To 0.1 mmol of resin-loaded peptide was added 0.2 mmol of N_3-PEG_4-COOH, 0.4 mmol of HCTU and 0.6 mmol of DIPEA in 3 mL DMF. The reaction was performed at room temperature for 5 hours. After thorough washing, 3 mL of 0.5 mmol trimethylphosphine in a 1,4-dioxane:H_2O (6:1) mixture was added to the resin (overnight reaction). Next, the peptide was reacted for 3 hours with cholesteryl hemisuccinate (0.3 mmol) in 3 mL DMF by the addition of HCTU (0.4 mmol) and DIPEA (0.6 mmol).

All peptides were cleaved from the resin using 3 mL of a TFA:triisopropylsilane: H_2O (95:2.5:2.5%) mixture and shaken for 1.5 hours. The peptides were precipitated by pouring the reaction mixture into 45 mL cold diethyl ether (-20 ℃) and isolated by centrifugation. The crude peptides were redissolved in H_2O (20 mL) and lyophilized.

For lipopeptide cleavage from the resin, 3 mL of a TFA:triisopropylsilane (97.5:2.5%) mixture was added and shaken for one hour. The crude lipopeptides were precipitated by pouring the reaction mixture into 45 ml of cold diethyl ether: n-hexane (1:1) and isolated by centrifugation. The pellet of the lipopeptides was redissolved in H_2O (20 mL) containing 10% acetonitrile and freeze-dried to yield a white powder.

Peptide purification

All peptides were purified with reversed-phase HPLC on a Shimazu system with two LC-8A pumps and an SPD-20A UV-Vis detector. A Kinetix Evo C18 column (21.2 mm diameter, 150 mm length, 5 μm particle size) was used for purification of all peptides. For the K_3, K_4, and K_5 peptides, a linear gradient from 20 to 45% acetonitrile in water (with 0.1% TFA) with a 12 mL/min flow rate over 28 mins was used. For the E_3, E_4, E_5 and fluo-E_4 peptides, a linear gradient from 20 to 55% was used. For lipopeptide purification, a Vydac C4 column (22 mm diameter, 250 mm length, 10 μm particle size) was used. All CPK lipopeptides were purified using a linear gradient from 20 to 65 % acetonitrile in water (with 0.1% TFA) with a 12 mL/min flow rate over 36 mins. All CPE lipopeptides were purified using a linear gradient from 20 to 75 % acetonitrile in water (with 0.1% TFA) with a 12

mL/min flow rate over 36 mins.

After HPLC purification, peptides were lyophilized yielding a white powder. The purity of all peptides was determined by LC-MS (Figure S7-S12, Table S1). The LC-MS results of CPK_3 and CPE_3 are shown in **chapter 2** of this thesis.

LC-MS analysis

LC-MS analysis was performed on a Thermo Scientific TSQ quantum access MAX mass detector connected to Ultimate 3000 liquid chromatography system fitted with a 50x4.6 mm Phenomenex Gemini 3 μm C18 column. LC-MS spectra were recorded using a linear gradient of 10-90% acetonitrile in H_2O with 0.1% TFA.

CD Spectroscopy

All CD measurements were performed on a JASCO J-815 CD spectrometer equipped with a Peltier temperature controller. All peptide stock solutions and measurement solutions were prepared in PBS. An 8 M GdnHCl stock solution was prepared in PBS. Unless otherwise specified, all CD measurements were performed at 20 ℃ in a 2 mm path length quartz cuvette. Datapoints were recorded from 190 nm to 260 nm wavelength with a 1 second response time and 2 nm bandwidth. The scanning speed was 200 nm/min and an average of five sequential spectra was recorded. For the concentration-dependent CD titration assay, the measurements were performed using a low sensitivity setting. Samples were prepared in a 1 mm path length quartz cuvette. All other parameters were the same as above. The initial concentration of each peptide was 250 μM and was diluted stepwise to 10 μM. For temperature-dependent CD measurements, the ellipticity at 222 nm was recorded from 5 ℃ to 90 ℃ at a rate of 60 ℃/h. Data points were recorded every 1 ℃ with a delay time of 3 seconds. The T_m was obtained by calculating the first-order derivative of the melting curve using the JASCO spectra analysis software, in which the melting temperature corresponded to the peak maximum of the first-order derivative of the melting curve.

All the spectra and melting curves were normalized to mean residue ellipticity using equation 1:

$$[\theta] = (1000 \times [\theta]_{obs})/(cnl) \quad (1)$$

Where $[\theta]$ represents the mean residue ellipticity in deg·cm^2·dmol^{-1}, $[\theta]_{obs}$ is the observed ellipticity in mdeg, c represents the peptide concentration in mM, n is the

number of amino acids in the peptide sequence and l represents the path length of the cuvette in mm.

The percentage of helicity of the peptides (F_{helix}) was calculated by equations 2 to 5:[47]

$$[\theta]_{max} = [\theta]_{\infty}(n - x)/n \quad (2)$$

$$[\theta]_{\infty} = (-44000 + 250T) \quad (3)$$

$$[\theta]_0 = 2220 - 53T \quad (4)$$

$$F_{helix} = 100\% \, ([\theta]_{222} - [\theta]_0) / ([\theta]_{max} - [\theta]_0) \quad (5)$$

In equation 2, $[\theta]_{max}$ is the maximum theoretical mean residue ellipticity, n is the number of the amino acids in the peptide sequence, x is the empirical constant which represents the number of amino acids that cannot contribute to the helicity due to the end fraying effect (usually between 2.4 to 4), for this work, x is 4. $[\theta]_{\infty}$ is the theoretical helicity of an infinite α-helix which can be calculated with equation (3). T is the temperature in ℃. $[\theta]_0$ is the mean residue ellipticity of the peptide when the peptide is in an entirely random coil conformation. $[\theta]_{\infty}$ and $[\theta]_0$ are temperature-dependent. $[\theta]_{222}$ represents the mean residue molar ellipticity of peptide at 222 nm.

The temperature-dependent CD was performed with the same instrument, using the same cuvette. Melting curves of all peptides were obtained by recording the ellipticity at 222 nm from 5 ℃ to 95 ℃ with a 1 ℃ data pitch and with a 60 ℃/h temperature ramp. The delay time for each data point was 2 seconds.

CD concentration-dependent titrations

Peptide monomers were dissolved in PBS at 250 μM and diluted gradually to lower concentrations (200 μM, 150 μM, 100 μM, 75 μM, 50 μM, 30 μM, 20 μM, 10 μM). Concentration-dependent CD spectra were recorded and the molar ellipticity at 222 nm was measured to calculate the helicity.

The nonlinear fitting and the peptide homodimerization calculation was obtained by employing the following equations:[40]

$$2P_m \leftrightarrow P_d \quad (6)$$

$$K_a = \frac{1}{K_d} \quad (7)$$

$$\mathrm{K_d} = \frac{[\mathrm{P_m}]^2}{[\mathrm{P_d}]} \quad (8)$$

$$[\mathrm{P_t}] = [\mathrm{P_m}] + 2[\mathrm{P_d}] \quad (9)$$

$$[\mathrm{P_t}] = [\mathrm{P_m}] + \frac{[\mathrm{P_m}]^2}{\mathrm{K_d}} \quad (10)$$

$$[P_m] = \frac{K_d}{4}\left(-1 + \sqrt{1 + \frac{8[P_t]}{K_d}}\right) \quad (11)$$

where $[\mathrm{P_m}]$ and $[\mathrm{P_d}]$ is the concentration of the monomeric and homodimeric peptide in mol/L. $[\mathrm{P_t}]$ is the total concentration of peptide in mol/L and $\mathrm{K_d}$ is the dissociation constant.

$$[\theta] = \frac{[\mathrm{P_m}][\theta_\mathrm{m}] + 2[\mathrm{P_d}][\theta_\mathrm{d}]}{\mathrm{P_t}} \quad (12)$$

$$[\theta] = \frac{[\mathrm{P_m}][\theta_\mathrm{m}] + \frac{2[\mathrm{P_m}]^2}{\mathrm{K_d}}[\theta_\mathrm{d}]}{\mathrm{P_t}} \quad (13)$$

$$[\theta] = \frac{\mathrm{K_d}\left(-1+\sqrt{1+\frac{8[\mathrm{P_t}]}{\mathrm{K_d}}}\right)\{2[\theta_\mathrm{m}] + \left(-1+\sqrt{1+\frac{8[\mathrm{P_t}]}{\mathrm{K_d}}}\right)[\theta_\mathrm{d}]\}}{8[\mathrm{P_t}]} \quad (14)$$

The normalized mean residue molar ellipticity can be calculated by equation 14, where $[\theta]$ represents the total normalized mean residue molar ellipticity at 222 nm wavelength, $[\theta_m]$ represents the normalized mean residue molar ellipticity contributed by the monomeric peptide and $[\theta_d]$ is the normalized mean residue molar ellipticity contributed by the homodimeric peptide. The non-linear binding curve can be fitted based on equation 14.

DLS

DLS measurements were recorded on a Zetasizer Nano S (Malvern Instruments, Malvern, UK) fitted with a green laser (532 nm). The derived count rate (DCR) measurements were performed using the non-invasive backscatter mode (automatic mode), detecting the scattered light at 175°. Room temperature measurements were recorded in a low volume cuvette (Brand, Wertheim, Germany) while temperature-dependent measurements were performed in a PCS8507 glass cuvette (Malvern). Temperature-dependent DLS data were collected from 20 ℃ to 90 ℃ and then

reversed from 90 ℃ to 20 ℃ at a rate of 1 ℃/min. Data points were recorded every 5 ℃ and all measurements were performed in duplicate.

UV-Vis

UV-Vis spectra were measured on an Agilent cary 300 spectrophotometer fitted with an Agilent temperature controller. Spectra were measured at 20 ℃ in a 1 cm quartz low-volume cuvette, using a scanning speed of 100 nm/min. Baseline correction was performed using the same solvent for sample preparation. The concentration of peptides for spectroscopy measurements are determined by using equation 15:

$$c = (A_{280} \times 10^6)/(5689 \times l) \quad (15)$$

Where c represents the concentration of mearsured peptide in μM, A_{280} represents the UV-Vis absorption at 280 nm, l is the path length of the cuvette in cm.

Lipid mixing and content mixing assays

Lipid mixing and content mixing assays were performed in black 96-well plates and the fluorescence change was recorded using a TECAN Infinite M1000 Pro microplate reader. A 10 mM lipid stock containing DOPC/DOPE/cholesterol (2:1:1) in $CHCl_3$/MeOH (1:1) was used for all liposome membrane fusion assays. All lipopeptides were dissolved in $CHCl_3$/MeOH (1:1) with a final concentration of 100 μM. DOPE-Nitrobenzoxadiazole (DOPE-NBD) and DOPE-Lissamine rhodamine B (DOPE-LrB) were dissolved in $CHCl_3$ with a final concentration of 1 mM.

For lipid mixing assays, four different batches of liposomes were prepared. Liposomes were prepared in 20 mL glass vials at [lipid] = 500 μM and 1 mL volume. For the first batch, a lipid film containing 99% lipids and 1% of lipopeptide K (CPK_3, CPK_4, and CPK_5) was used. For the second batch, the lipid film contained 98% lipids, 0.5% DOPE-NBD, 0.5% DOPE-LrB and 1% lipopeptide E (CPE_3, CPE_4 and CPE_5). The third batch contained 99.5% lipids, 0.25% DOPE-NBD and 0.25% DOPE-LrB. Plain liposomes were also prepared as a control sample. All lipid films were dried under N_2 for 2 hours, followed by

vacuum desiccation for 30 mins. Lipid films were rehydrated with 1 mL PBS, vortexed for 30 seconds and sonicated at 55 ℃ for 3 mins in a Branson 2510 bath sonicator. The quality of the liposomes (size and polydispersity) was assessed by DLS. Liposome with a hydrodynamic diameter of 100 nm with a PDI < 0.3 were used in the lipid- and content-mixing assays. All liposomes were diluted to [total lipid] = 200 μM before use.

For the lipid-mixing assays, 100 μL of liposomes from batch 1 were mixed with 100 μL of liposomes from batch 2 and the NBD emission at 530 nm was measured over time immediately after mixing. 200 μL of liposomes from batch 3 were used as the positive control, which contains the same amount of NBD/LrB but in double the amount of liposomes. The negative control for the assay was prepared by mixing 100 μL of liposomes from batch 2 with 100 μL of free liposomes. The experiment was performed in triplicate with liposomes from the same batch and repeated at least twice with liposomes from different batches. The lipid mixing efficiency was calculated using equation 16.

$$\%F_t = 100\% \times (F_t - F_0)/(F_{max} - F_0) \quad (16)$$

Where F_t represents the real-time fluorescence intensity, F_0 and F_{max} are the fluorescence intensity from the negative control and positive control respectively at the same time point.

Content mixing was performed in a similar manner. Three batches of liposomes were prepared. Batch 1 liposomes contained 99% lipid and 1% CPK_n. Batch 2 liposomes contained 99% lipid and 1% CPE_n and these are loaded with 20 mM Sulforhodamine B (SrB) . Batch 3 liposomes contained 99% lipid and 1% CPE_n and these were loaded with 10 mM Srb. Plain liposomes were prepared for control experiments. All batches of liposomes were prepared using the sonication method at [total lipid] = 500 μM. SRb liposomes were purified using a Illustra NAP-25 size-exclusion column to remove the non-encapsulated dye. All liposomes were diluted to [lipid] = 200 μM before use. The assay was performed by mixing 100 μL of liposomes from batch 1 and 100 μL of liposomes from batch 2 while measuring SRb emission at 585 nm. Batch 3 liposomes were used as the positive control. As negative control, 100 μL of liposomes from batch 2 were mixed with 100 μL of plain liposomes. The experiment was performed in triplicate with liposomes from the same batch and repeated at least twice with liposomes from different batches. The content mixing efficiency was calculated with equation 15.

Membrane labelling

100 μL CPK_n (100 μM in $CHCl_3$/MeOH (1:1) was transferred to a 20 mL glass vial and dried to a film under an N_2 flow, followed by drying in a vacuum desiccator for 30 mins. 1 mL of DMEM (with 10% of FCS) was added and sonicated for five minutes, resulting in lipopeptide micelles.

Hela cells were seeded in an μ-Slide 8 Well with a cell number of $5x10^4$ cells per well for 20 hours. CPK_n micelles (200 μM) were added to each well and incubated at 37 ℃ for 1.5 h. The cells were washed with DMEM three times before 200 μL of fluo-E_4 (10 μM in DMEM) was added and incubated at 37 ℃ for 10 min. A well of non-lipopeptide K treated cells was also incubated with fluo-E_4 as the negative control. After incubation, free fluo-E_4 was removed and the cells were washed at least three times with DMEM before imaging. Cell imaging was performed with a Leica SP8 confocal microscopy. A 488nm laser was used for excitation and the emission signal was collected from 500 nm to 550 nm.

Membrane Docking

Hela cells were seeded in a 48-well plate with a cell number of $1x10^5$ cells per well and incubated at 37 ℃ for 20 h. CPK_n micelles in DMEM were prepared using the same method as above. 400 μL of each micelle solution was added to each well plate and incubated with the cells at 37 ℃ for 1.5 h. 500 μM of liposomes containing 1% CPE_n and 1% DOPE-NBD were prepared. For the control experiment, plain liposomes containing 1% DOPE-NBD were used. The liposomes were diluted to [total lipid] = 200 μM in DMEM before addition to cells. After 15 minutes of incubation, the cells were washed three times with DMEM, followed by the addition of 400 μL liposome solution with CPE_n. Control experiment: CPK decorated cells with non-CPE liposomes and non-CPK decorated cells with CPE-modified liposomes were used. Cells were incubated with the liposomes for 15 min at 37 ℃ before thoroughly washing with PBS. Cells were trypsinized and transferred to Eppendorf tubes, washed with PBS and centrifuged. The cells were resuspended in PBS (supplemented with 2 mM EDTA) to a density of $5x10^5$ cells/mL and transferred to a 96-well plate for FACS measurements using a Guava® EasyCyte 12HT Benchtop Flow Cytometer. The data were analyzed using FlowJo v10. For each measurement, 10,000 events in duplicate were collected. No compensation was required for the fluorophores used.

PI-NBD delivery through membrane fusion

$5x10^4$ Hela cells were seeded in each well of two µ-Slide 8 Well plates and incubated at 37 ℃ for 20 hours. A 10 µM solution of CPK_n in DMEM was prepared as described above. A lipid film ([Total lipid] = 1 mmol) containing 1% CPE_n and 1% DOPE-NBD was rehydrated with 1 mL of a PI (10 mg/mL) solution in PBS and sonicated five minutes at 55 ℃ to obtain liposomes. Non-encapsulated PI was removed using an Illustra NAP-25 size-exclusion column. For comparison, liposomes containing DOPE-NBD and PI but without CPE were also prepared. All liposomes were diluted with DMEM to a final lipid concentration of 200 µM. 200 µL of CPK_n micelles (10 µM) were added to the cells and incubated for 1.5 h at 37 ℃. After thorough washing, liposomes (200 µL) were added to the cells for 15 mins. Control experiments: liposomes without CPE + cells decorated with CPK, and liposomes with CPE + cells without CPK were used. After incubation, excess liposomes were removed and the cells were washed with DMEM. The cells were covered with fresh DMEM and incubated at 37 ℃ for another 20 mins before imaging.

Cell imaging was performed using a Leica SP8 confocal microscope. A 488 nm laser was applied for excitation and NBD emission was observed in the range from 500 to 550 nm. For PI observation, a 535 nm laser was used for excitation and emission was measured from 600 nm to 700 nm.

REFERENCES

(1) Elsharkasy, O. M.; Nordin, J. Z.; Hagey, D. W.; de Jong, O. G.; Schiffelers, R. M.; Andaloussi, S. E.; Vader, P. Extracellular vesicles as drug delivery systems: Why and how? *Adv Drug Deliv Rev* **2020,** *159*, 332.

(2) Su, Y.-Y.; Li, C.-Y.; Li, D. Progress in Membrane Fusion and Its Application in Drug Delivery. *Chinese Journal of Analytical Chemistry* **2019,** *47*, 1871.

(3) Yang, J.; Bahreman, A.; Daudey, G.; Bussmann, J.; Olsthoorn, R. C.; Kros, A. Drug Delivery via Cell Membrane Fusion Using Lipopeptide Modified Liposomes. *ACS Cent Sci* **2016,** *2*, 621.

(4) Brock, D. J.; Kustigian, L.; Jiang, M.; Graham, K.; Wang, T. Y.; Erazo-Oliveras, A.; Najjar, K.; Zhang, J.; Rye, H.; Pellois, J. P. Efficient cell delivery mediated by lipid-specific endosomal escape of supercharged branched peptides. *Traffic* **2018,** *19*, 421.

(5) Gilleron, J.; Querbes, W.; Zeigerer, A.; Borodovsky, A.; Marsico, G.; Schubert, U.; Manygoats, K.; Seifert, S.; Andree, C.; Stoter, M.; Epstein-Barash, H.; Zhang, L.; Koteliansky, V.; Fitzgerald, K.; Fava, E.; Bickle, M.; Kalaidzidis, Y.; Akinc, A.; Maier, M.; Zerial, M. Image-based analysis of lipid

nanoparticle-mediated siRNA delivery, intracellular trafficking and endosomal escape. *Nat Biotechnol* **2013,** *31*, 638.

(6) Sahay, G.; Querbes, W.; Alabi, C.; Eltoukhy, A.; Sarkar, S.; Zurenko, C.; Karagiannis, E.; Love, K.; Chen, D.; Zoncu, R.; Buganim, Y.; Schroeder, A.; Langer, R.; Anderson, D. G. Efficiency of siRNA delivery by lipid nanoparticles is limited by endocytic recycling. *Nat Biotechnol* **2013,** *31*, 653.

(7) Chernomordik, L. V.; Kozlov, M. M. Mechanics of membrane fusion. *Nat Struct Mol Biol* **2008,** *15*, 675.

(8) Byrne, R. D.; Veeriah, S.; Applebee, C. J.; Larijani, B. Conservation of proteo-lipid nuclear membrane fusion machinery during early embryogenesis. *Nucleus* **2014,** *5*, 441.

(9) Jantsch-Plunger, V.; Glotzer, M. Depletion of syntaxins in the early Caenorhabditis elegans embryo reveals a role for membrane fusion events in cytokinesis. *Current biology* **1999,** *9*, 738.

(10) Paululat, A.; Holz, A.; Renkawitz-Pohl, R. Essential genes for myoblast fusion in Drosophila embryogenesis. *Mechanisms of development* **1999,** *83*, 17.

(11) Scales, S. J.; Chen, Y. A.; Yoo, B. Y.; Patel, S. M.; Doung, Y.-C.; Scheller, R. H. SNAREs contribute to the specificity of membrane fusion. *Neuron* **2000,** *26*, 457.

(12) Wang, Y.; Li, L.; Hou, C.; Lai, Y.; Long, J.; Liu, J.; Zhong, Q.; Diao, J. SNARE-mediated membrane fusion in autophagy. *Semin Cell Dev Biol* **2016,** *60*, 97.

(13) Harrison, S. C. Viral membrane fusion. *Nat Struct Mol Biol* **2008,** *15*, 690.

(14) Tang, T.; Bidon, M.; Jaimes, J. A.; Whittaker, G. R.; Daniel, S. Coronavirus membrane fusion mechanism offers a potential target for antiviral development. *Antiviral Res* **2020,** *178*, 104792.

(15) Harrison, S. C. Viral membrane fusion. *Virology* **2015,** *479-480*, 498.

(16) Whitehead, S. A.; McNitt, C. D.; Mattern-Schain, S. I.; Carr, A. J.; Alam, S.; Popik, V. V.; Best, M. D. Artificial Membrane Fusion Triggered by Strain-Promoted Alkyne-Azide Cycloaddition. *Bioconjug Chem* **2017,** *28*, 923.

(17) Ma, M.; Bong, D. Controlled fusion of synthetic lipid membrane vesicles. *Accounts of chemical research* **2013,** *46*, 2988.

(18) Stengel, G.; Simonsson, L.; Campbell, R. A.; Höök, F. Determinants for membrane fusion induced by cholesterol-modified DNA zippers. *The Journal of Physical Chemistry B* **2008,** *112*, 8264.

(19) Sun, L.; Gao, Y.; Wang, Y.; Wei, Q.; Shi, J.; Chen, N.; Li, D.; Fan, C. Guiding protein delivery into live cells using DNA-programmed membrane fusion. *Chem Sci* **2018,** *9*, 5967.

(20) Mason, J. M.; Arndt, K. M. Coiled coil domains: stability, specificity, and biological implications. *Chembiochem* **2004,** *5*, 170.

(21) Apostolovic, B.; Danial, M.; Klok, H. A. Coiled coils: attractive protein folding motifs for the fabrication of self-assembled, responsive and bioactive materials. *Chem Soc Rev* **2010,** *39*, 3541.

(22) Conticello, V.; Hughes, S.; Modlin, C. Biomaterials made from coiled-coil peptides. *Fibrous Proteins: Structures and Mechanisms* **2017,** 575.

(23) Wu, Y.; Collier, J. H. α‐Helical coiled‐coil peptide materials for biomedical applications. *Wiley Interdisciplinary Reviews: Nanomedicine and Nanobiotechnology* **2017,** *9*, e1424.

(24) Woolfson, D. N. Building fibrous biomaterials from alpha-helical and collagen-like coiled-coil peptides. *Biopolymers* **2010,** *94*, 118.

(25) Fletcher, N. L.; Lockett, C. V.; Dexter, A. F. A pH-responsive coiled-coil peptide hydrogel. *Soft Matter* **2011,** *7*, 10210.

(26) Wu, Y.; Collier, J. H. alpha-Helical coiled-coil peptide materials for biomedical applications. *Wiley Interdiscip Rev Nanomed Nanobiotechnol* **2017,** *9*.

(27) Hill, L. K.; Meleties, M.; Katyal, P.; Xie, X.; Delgado-Fukushima, E.; Jihad, T.; Liu, C. F.; O'Neill, S.; Tu, R. S.; Renfrew, P. D.; Bonneau, R.; Wadghiri, Y. Z.; Montclare, J. K. Thermoresponsive Protein-Engineered Coiled-Coil Hydrogel for Sustained Small Molecule Release. *Biomacromolecules* **2019,** *20*, 3340.

(28) Lin, Y.; An, B.; Bagheri, M.; Wang, Q.; Harden, J. L.; Kaplan, D. L. Electrochemically Directed Assembly of Designer Coiled-Coil Telechelic Proteins. *ACS Biomater Sci Eng* **2017,** *3*, 3195.

(29) Marsden, H. R.; Tomatsu, I.; Kros, A. Model systems for membrane fusion. *Chemical Society Reviews* **2011,** *40*, 1572.

(30) Versluis, F.; Voskuhl, J.; van Kolck, B.; Zope, H.; Bremmer, M.; Albregtse, T.; Kros, A. In situ modification of plain liposomes with lipidated coiled coil forming peptides induces membrane fusion. *J Am Chem Soc* **2013,** *135*, 8057.

(31) Zheng, T.; Voskuhl, J.; Versluis, F.; Zope, H. R.; Tomatsu, I.; Marsden, H. R.; Kros, A. Controlling the rate of coiled coil driven membrane fusion. *Chem Commun (Camb)* **2013,** *49*, 3649.

(32) Zope, H. R.; Versluis, F.; Ordas, A.; Voskuhl, J.; Spaink, H. P.; Kros, A. In vitro and in vivo supramolecular modification of biomembranes using a lipidated coiled-coil motif. *Angew Chem Int Ed Engl* **2013,** *52*, 14247.

(33) Yang, J.; Shimada, Y.; Olsthoorn, R. C.; Snaar-Jagalska, B. E.; Spaink, H. P.; Kros, A. Application of Coiled Coil Peptides in Liposomal Anticancer Drug Delivery Using a Zebrafish Xenograft Model. *ACS Nano* **2016,** *10*, 7428.

(34) Kong, L.; Askes, S. H.; Bonnet, S.; Kros, A.; Campbell, F. Temporal control of membrane fusion through photolabile PEGylation of liposome membranes. *Angewandte Chemie* **2016,** *128*, 1418.

(35) Litowski, J. R.; Hodges, R. S. Designing heterodimeric two-stranded alpha-helical coiled-coils. Effects of hydrophobicity and alpha-helical propensity on protein folding, stability, and specificity. *J Biol Chem* **2002,** *277*, 37272.

(36) Rabe, M.; Boyle, A.; Zope, H. R.; Versluis, F.; Kros, A. Determination of oligomeric states of peptide complexes using thermal unfolding curves. *Biopolymers* **2015,** *104*, 65.

(37) Paulucci, A. A.; Hicks, L.; Machado, A.; Miranda, M. T.; Kay, C. M.; Farah, C. S. Specific sequences determine the stability and cooperativity of folding of the C-terminal half of tropomyosin. *J Biol Chem* **2002,** *277*, 39574.

(38) Crooks, R. O.; Rao, T.; Mason, J. M. Truncation, randomization, and selection: generation of a reduced length c-Jun antagonist that retains high interaction stability. *J Biol Chem* **2011,** *286*, 29470.

(39) Kumar, P.; van Son, M.; Zheng, T.; Valdink, D.; Raap, J.; Kros, A.; Huber, M. Coiled-coil formation of the membrane-fusion K/E peptides viewed by electron paramagnetic resonance. *PLOS ONE* **2018,** *13*, e0191197.

(40) Crone, N. S. A.; Kros, A.; Boyle, A. L. Modulation of Coiled-Coil Binding Strength and Fusogenicity through Peptide Stapling. *Bioconjug Chem* **2020,** *31*, 834.

(41) Monera, O. D.; Kay, C. M.; Hodges, R. S. Protein denaturation with guanidine hydrochloride or urea provides a different estimate of stability depending on the contributions of electrostatic interactions. *Protein Science* **1994,** *3*, 1984.

(42) Lim, W. K.; Rosgen, J.; Englander, S. W. Urea, but not guanidinium, destabilizes proteins by forming hydrogen bonds to the peptide group. *Proc Natl Acad Sci U S A* **2009,** *106*, 2595.

(43) Huerta-Viga, A.; Woutersen, S. Protein Denaturation with Guanidinium: A 2D-IR Study. *J Phys Chem Lett* **2013,** *4*, 3397.

(44) Daudey, G. A.; Zope, H. R.; Voskuhl, J.; Kros, A.; Boyle, A. L. Membrane-Fusogen Distance Is Critical for Efficient Coiled-Coil-Peptide-Mediated Liposome Fusion. *Langmuir* **2017,** *33*, 12443.

(45) Rabe, M.; Schwieger, C.; Zope, H. R.; Versluis, F.; Kros, A. Membrane interactions of fusogenic coiled-coil peptides: implications for lipopeptide mediated vesicle fusion. *Langmuir* **2014,** *30*, 7724.

(46) Rabe, M.; Aisenbrey, C.; Pluhackova, K.; de Wert, V.; Boyle, A. L.; Bruggeman, D. F.; Kirsch, S. A.; Bockmann, R. A.; Kros, A.; Raap, J.; Bechinger, B. A Coiled-Coil Peptide Shaping Lipid Bilayers upon Fusion. *Biophys J* **2016,** *111*, 2162.

(47) de Araujo, A. D.; Hoang, H. N.; Kok, W. M.; Diness, F.; Gupta, P.; Hill, T. A.; Driver, R. W.; Price, D. A.; Liras, S.; Fairlie, D. P. Comparative α‐Helicity of Cyclic Pentapeptides in Water. *Angewandte Chemie International Edition* **2014,** *53*, 6965.

APPENDIX 3

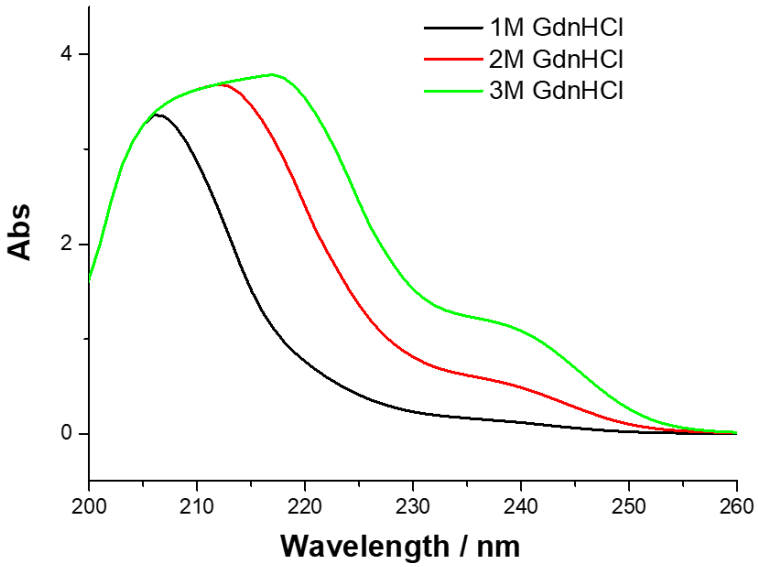

Figure S1. UV-Vis spectra of different concentrations of GdnHCl in PBS.

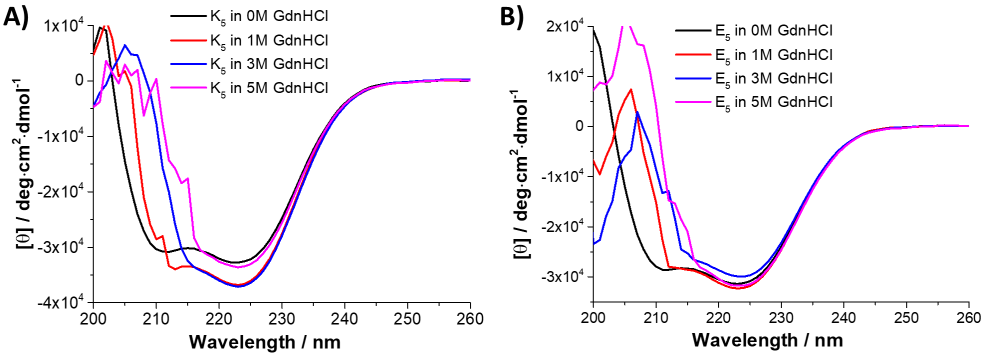

Figure S2. CD spectra of peptides K_5 (A) and E_5 (B) with different concentrations of GdnHCl. Peptide: 10 μM, temperature: 20 °C.

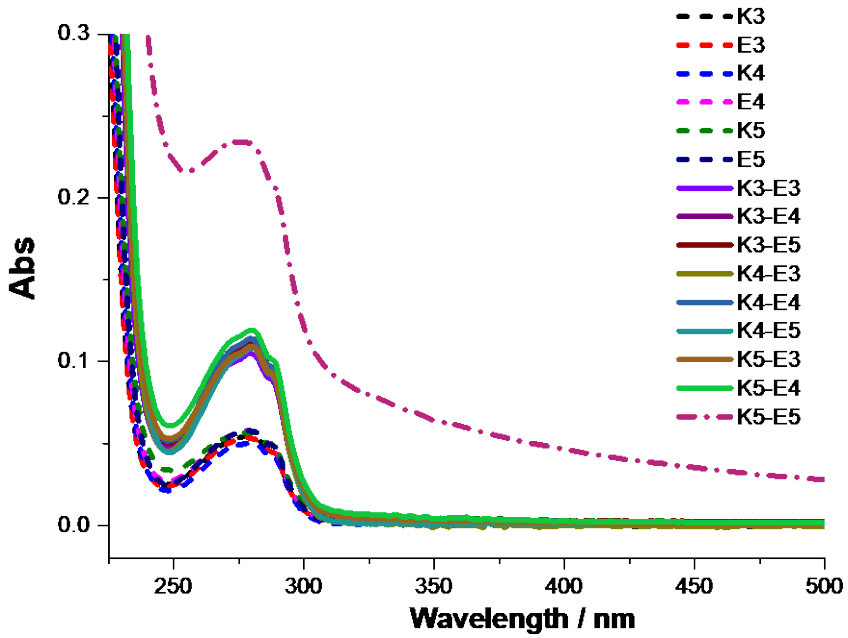

Figure S3. UV-Vis spectra of different coiled-coil forming peptides and coiled-coil pairs. A baseline shift was obtained for the K_5-E_5 coiled coil pair, indicative of aggregation. All measurements were recorded in PBS (pH 7.2) at 20 °C. Peptide: 10 µM.

A) Lipid mixing:

Lipid mixing efficiency with reference to peptide E:

K5E4 > K4E4 > K4E5 > K5E5 = K3E4 = K3E5 > K5E3 = K4E3 > K3E3

E4>E5>E3

Lipid mixing efficiency with reference to peptide K:

K5E4 > K4E4 > K4E5 > K5E5 = K3E4 = K3E5 > K5E3 = K4E3 > K3E3

K5>K4>K3

B) Content mixing:

Content mixing efficiency with reference to peptide E :

K5E4 > K4E4 > K3E4 > K5E3 = K4E3 = K5E5 > K4E5 = K3E3 = K3E5

E4>E3>E5

Content mixing efficiency with reference to peptide K :

K5E4 > K4E4 > K3E4 > K5E3 = K4E3 = K5E5 > K4E5 = K3E3 = K3E5

K5>K4>K3

Figure S4. Comparison of liposome membrane fusion efficiency for different length E and K peptides.

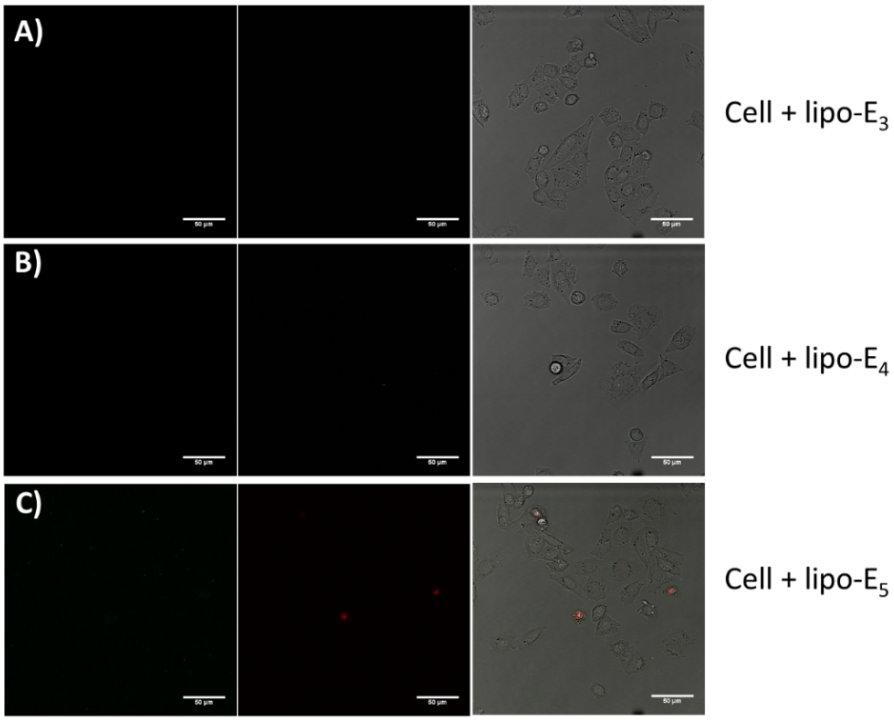

Figure S5. Non-CPK decorated cells incubated with CPE-modified liposomes containing PI and NBD-PE. Scale bar: 50 μm.

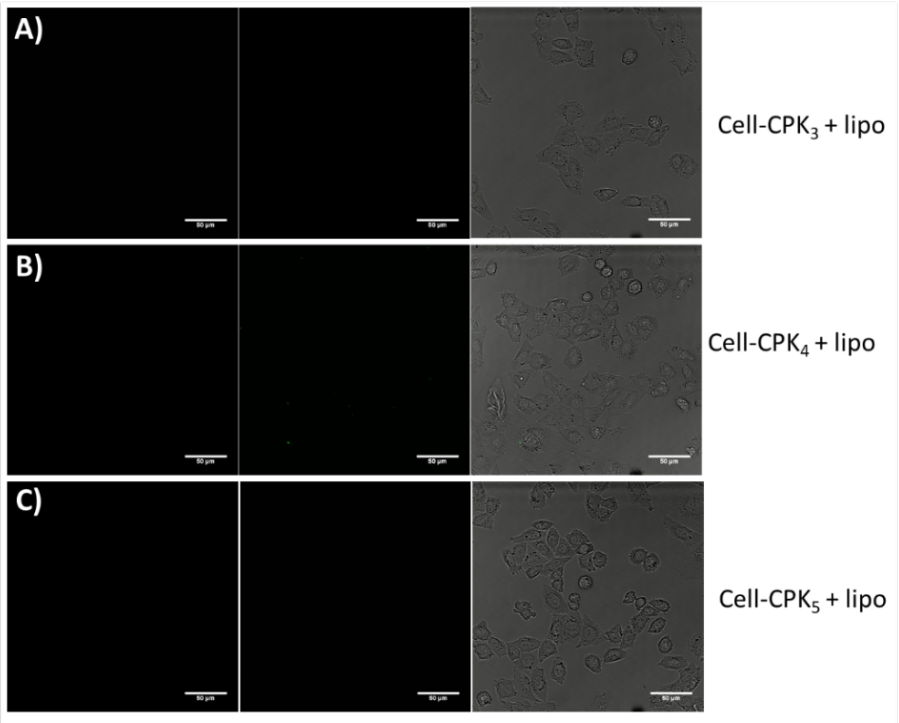

Figure S6. CPK-decorated cells incubated with non-CPE modified liposomes containing PI and NBD-PE. Scale bar: 50 µm.

Table S1. Calculated mass and recorded mass by LC-MS for all peptides and lipopeptides.

peptide	Mass (calcd.) / Da	Mass (found) / Da
K_3	$[M + 2H^+]^{2+}$ 1282.8	1281.5
E_3	$[M + H^+]^{+}$ 1284.2	1283.0
K_4	$[M + 2H^+]^{2+}$ 1659.5	1658.5
	$[M + 3H^+]^{3+}$ 1106.6	1105.5
E_4	$[M + 2H^+]^{2+}$ 1161.4	1660.5
	$[M + 3H^+]^{3+}$ 1107.9	1106.7
K_5	$[M + 3H^+]^{3+}$ 1359.0	1357.0
E_5	$[M + 3H^+]^{3+}$ 1360.6	1358.4
CPK_4	$[M + 2H^+]^{2+}$ 1869.4	1866.4
	$[M + 3H^+]^{3+}$ 1246.6	1244.3
CPE_4	$[M + 2H^+]^{2+}$ 1871.2	1868.8
	$[M + 3H^+]^{3+}$ 1247.8	1245.4
CPK_5	$[M + 2H^+]^{2+}$ 2245.5	2244.6
	$[M + 3H^+]^{3+}$ 1497.3	1495.5
	$[M + 4H^+]^{4+}$ 1123.2	1121.5
CPE_5	$[M + 2H^+]^{2+}$ 2246.3	2247.0
	$[M + 3H^+]^{3+}$ 1497.9	1497.3
Fluo-K_4	$[M + 2H^+]^{2+}$ 1876.5	1874.0
	$[M + 3H^+]^{3+}$ 1251.3	1249.3
Fluo-E_4	$[M + 2H^+]^{2+}$ 1878.5	1876.0
	$[M + 3H^+]^{3+}$ 1252.7	1250.6

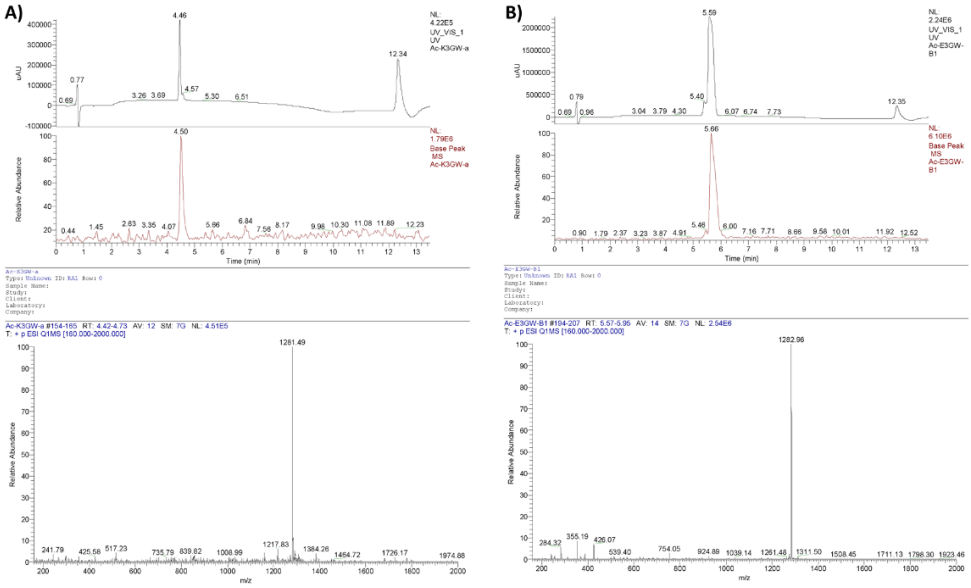

Figure S7. LC-MS of: A) K_3 and B) E_3.

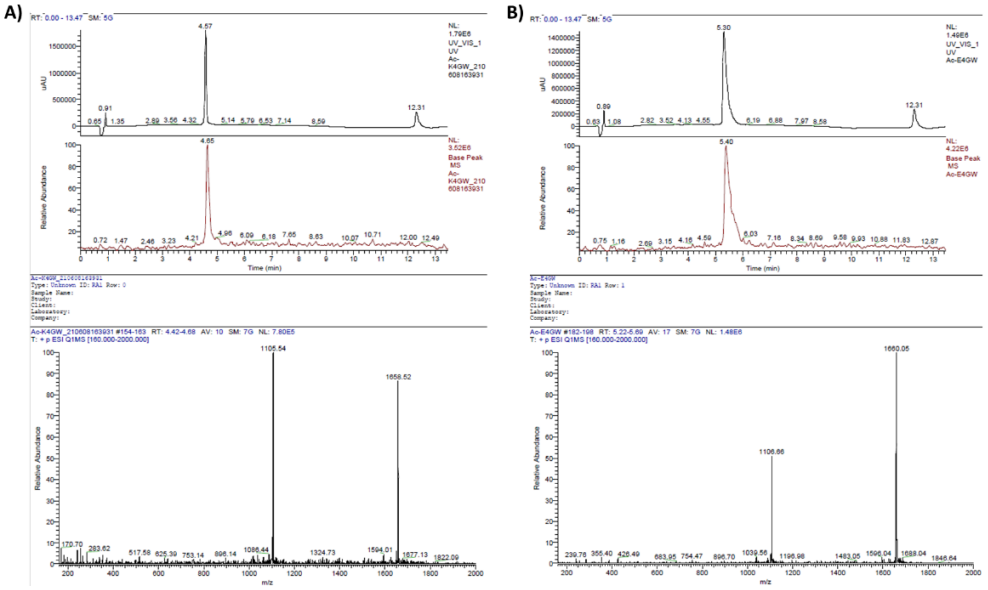

Figure S8. LC-MS of: A) K_4 and B) E_4.

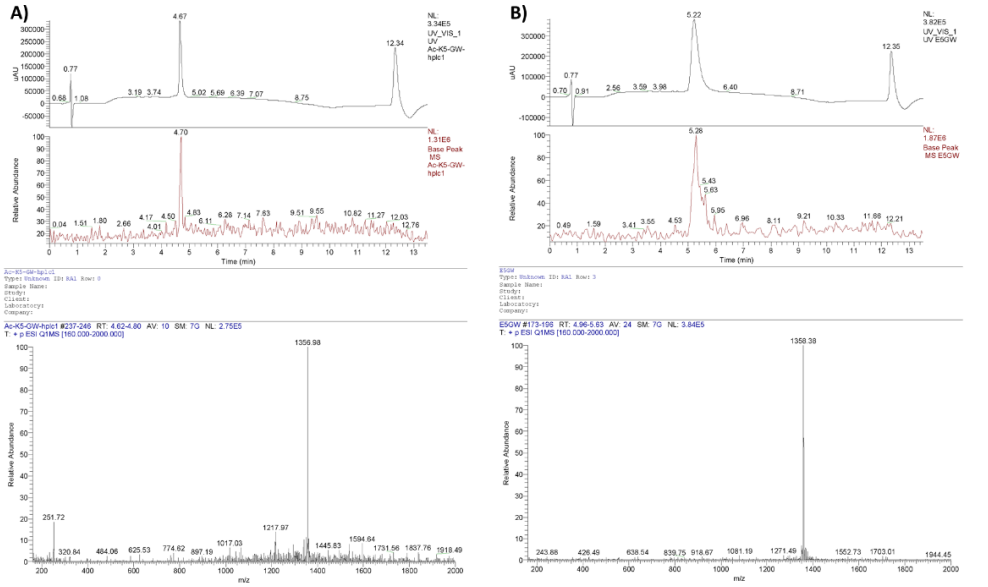

Figure S9. LC-MS of: A) K_5 and B) E_5.

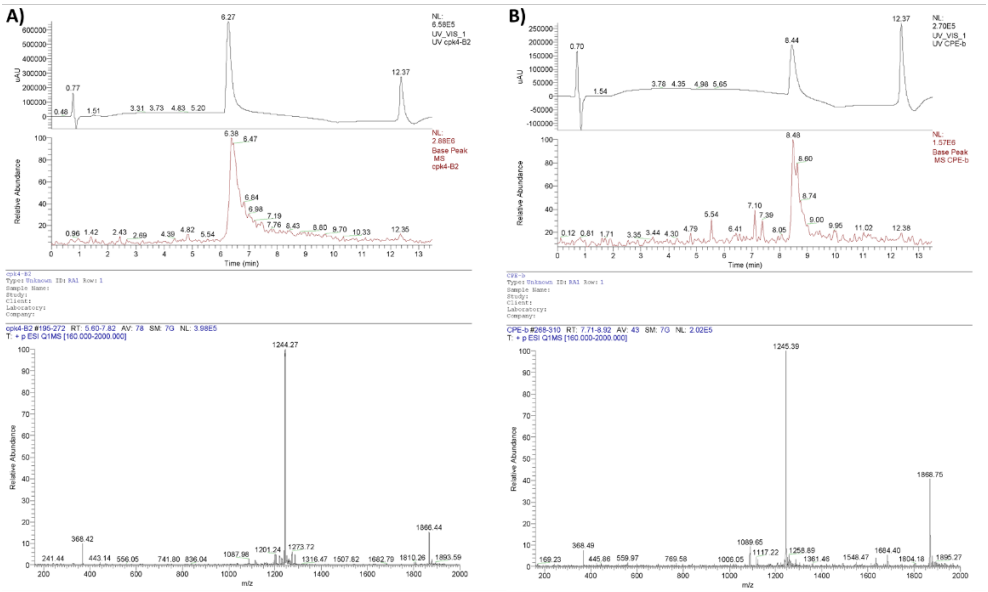

Figure S10. LC-MS of: A) CPK_4 and B) CPE_4.

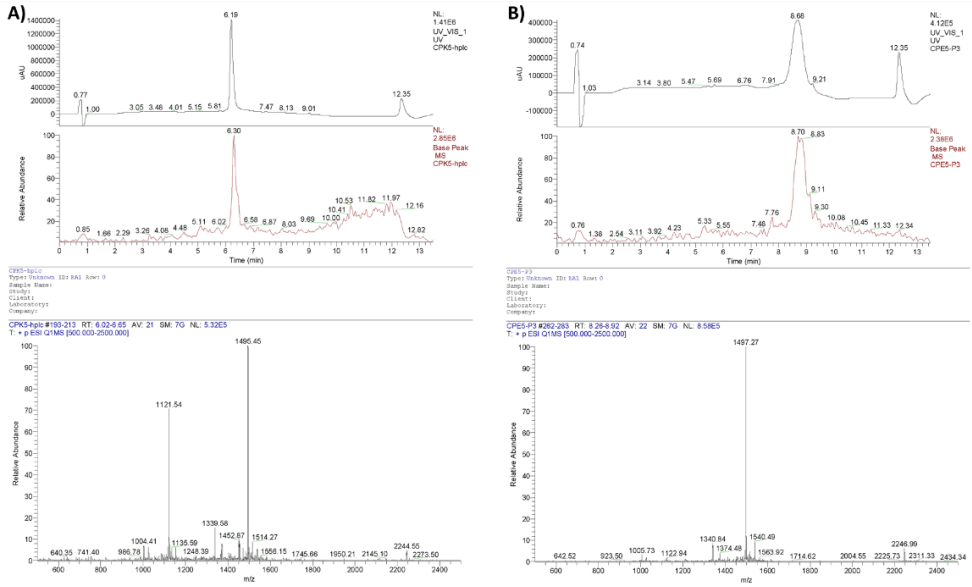

Figure S11. LC-MS of: A) CPK_5 and B) CPE_5.

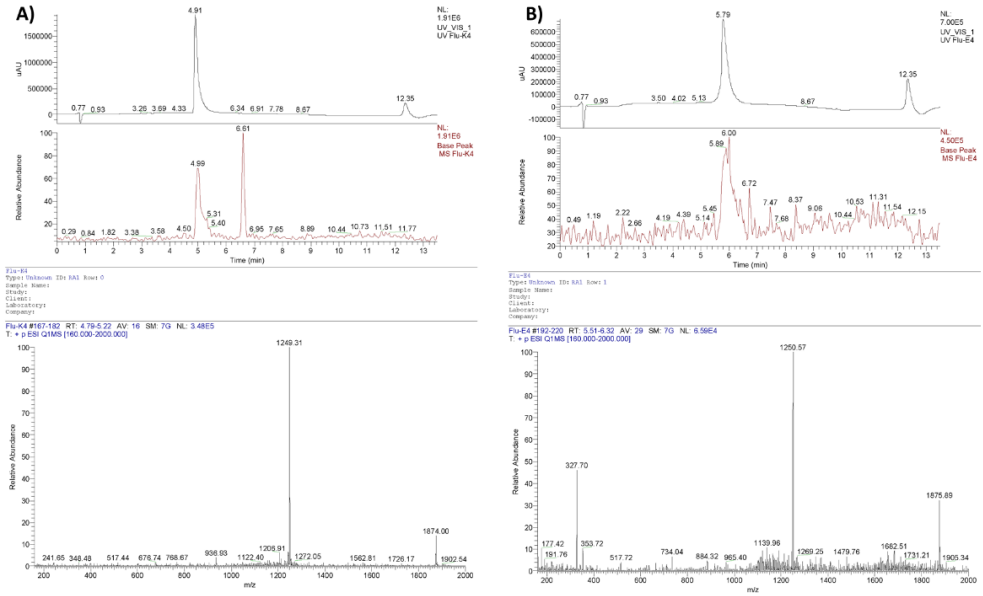

Figure S12. LC-MS of: A) fluo-K_4 and B) fluo-E_4.